https://doi.org/10.5194/egusphere-2026-3416
Preprint. Discussion started: 19 June 2026

Cleaner air, drier land: the unintended drought consequences of near-term climate forcers mitigation

Tianhui Zhou[1], Massimo A. Bollasina[1], and David Stevenson[1]

[1]School of GeoSciences, University of Edinburgh, Edinburgh, UK

Correspondence to: Tianhui Zhou (T.Zhou-16@sms.ed.ac.uk)

Abstract. Drought poses severe threats to water resources, ecosystems, and socioeconomic well-being worldwide. While greenhouse gas (GHG) emissions are the primary driver of global warming and the associated intensification of the hydrological cycle, the role of non-methane near-term climate forcers (NTCFs) — encompassing aerosols and their precursors, ozone-forming reactive gases, and other short-lived species — in modulating regional drought risk remains poorly constrained, particularly in arid and semi-arid regions where aerosol-induced radiative effects and circulation feedbacks interact non-linearly with the water balance. Here we employ seven Earth System Models from the CMIP6 AerChemMIP framework to quantify the contribution of NTCF emissions to drought evolution under two future pathways that share identical GHG forcing but differ in the stringency of NTCF controls: SSP3-7.0 and SSP3-7.0-lowNTCF. Using the Standardised Precipitation Evapotranspiration Index at 3-, 6-, and 12-month timescales, we characterise projected changes in drought frequency, duration, intensity, and severity by mid-21st century and identify the large-scale dynamical mechanisms driving regional responses. NTCF mitigation exerts negligible influence on global-mean drought tendency but produces strongly heterogeneous regional responses, with drought conditions worsening substantially across the Sahel, West Asia, Central Asia, and the Mediterranean, while Southeast Asia, Australia, and Central America experience significant drought reductions. These findings are robust across the majority of models and highlight that air quality policies carry regionally differentiated and sometimes counterintuitive hydrological consequences that must be considered alongside their climate and health co-benefits.

1 Introduction

Droughts are climate anomalies characterised by prolonged (months to years) deficits in precipitation and soil moisture, with severe consequences for human health, ecosystems and socio-economic activities (Wilhite and Glantz, 1985; Trenberth et al., 2014). To capture their multifaceted nature, droughts are commonly classified into four categories: meteorological, hydrological, agricultural, and socio-economic (Lynch et al., 2020). In regions already highly-vulnerable to climate change and hydroclimate variability, recent drought events have caused widespread disruption. The 2011–2017 California drought resulted in cumulative economic losses exceeding $3 billion and triggered severe groundwater depletion (Howitt et al., 2015). Globally, between 1995 and 2015, approximately 1.1 billion people were affected by droughts (UNISDR and CRED, 2015). As global temperatures rise and precipitation patterns shift, the frequency and intensity of drought events are projected to

https://doi.org/10.5194/egusphere-2026-3416
Preprint. Discussion started: 19 June 2026

intensify further under continued warming, albeit with strong regional heterogeneity (Ebi et al., 2021). Developing a better understanding of the drivers of future drought variability, including the respective roles of internal climate variability and anthropogenic forcing, and the underpinning physical mechanisms, is therefore critical for informing climate adaptation and water resource management (Cook et al., 2018; Diffenbaugh et al., 2015).

Although the continued increase in well-mixed greenhouse gases (GHGs) is recognised as the primary driver of long-term global warming and associated changes in the hydrological cycle (Held and Soden, 2006; Allen et al., 2020), other factors can play an important role, particularly at regional scales and over short- to medium-term time horizons. Near-term climate forcers (NTCFs), often co-emitted with GHGs, include aerosols and their precursor gases, such as sulfur dioxide (SO_2), organic carbon (OC) and black carbon (BC), as well as chemically reactive gases including ozone (O_3) and methane (CH_4), both of which are important but relatively short-lived GHGs. Unlike long-lived GHGs, NTCFs affect climate on timescales of weeks to a decade (Myhre et al., 2013). Despite their short lifetimes, NTCFs perturb the Earth's radiative balance with a net radiative forcing on climate that is comparable in magnitude to that of CO_2 (Myhre et al., 2013; Shindell et al., 2012), though with substantial differences in sign and magnitude across individual species (Boucher et al., 2013).

Reductions in non-absorbing aerosols tend to warm the climate system, whereas reductions in absorbing aerosols, tropospheric ozone, and methane lead to cooling. Beyond their direct radiative effects, changes in NTCFs influence precipitation patterns through modifications to atmospheric stability, large-scale circulation, and cloud–precipitation processes. For instance, the growth of anthropogenic aerosol emissions during the 20th century has been linked to reduced global mean precipitation, partially offsetting GHG-driven increases (Wu et al., 2013; Salzmann, 2016; Richardson et al., 2018). The interhemispheric contrast in aerosol forcing has also likely contributed to a southward shift of the tropical rain belt (e.g., Chung and Soden, 2017). At regional scales, aerosols have been identified as key contributors to the weakening of the West African monsoon and the Sahel drought in the mid-1980s, as well as to the observed decline in South and East Asian monsoon precipitation during the second half of the 20th century (e.g., Bollasina et al., 2011; Polson et al., 2014; Song et al., 2014; Undorf et al., 2018; Liu et al., 2019; Zhang et al., 2022; Liu et al., 2024). In the case of absorbing aerosols, particularly within the boundary layer, atmospheric heating stabilises the lower troposphere, suppresses convection, and reduces precipitation (Ming et al., 2010; Ban-Weiss et al., 2012; Stjern et al., 2017; Allen et al.,2021). Ozone and its precursors can further exacerbate drying by enhancing the greenhouse effect and increasing surface temperatures (Naimark et al., 2021; Lei et al., 2022).

In addition to their climatic impacts, NTCFs are major contributors to ambient air pollution, including surface O_3 and fine particulate matter ($PM_{2.5}$). Air pollution caused approximately 8.1 million premature deaths globally in 2021, with about half due to outdoor air pollution (Lelieveld et al., 2023; GBD 2021 Risk Factors Collaborators, 2024). Mitigating NTCFs is therefore critical not only for climate but also for advancing the United Nations Sustainable Development Goals and the

https://doi.org/10.5194/egusphere-2026-3416
Preprint. Discussion started: 19 June 2026

objectives of the Paris Agreement, with integrated mitigation strategies offering substantial co-benefits for public health, food security, and economic welfare (e.g., Shindell et al., 2012; Haines et al., 2017).

Currently, NTCF emissions are concentrated in densely populated and industrialised regions, including China, India, eastern North America, and Europe (Hoesly et al., 2018), with Africa also a major source of black and organic carbon aerosols due to widespread biomass burning. Since around 2000, Eastern and Southern Asia have exhibited the highest NTCF emissions, driven by rapid industrialisation (Szopa et al., 2021), while emissions in North America and Europe have declined due to stringent air-quality regulations (Aas et al., 2019; Miyazaki et al., 2017). These trends, including a sharp reduction in Chinese SO_2 emissions from the 2010s (Zheng et al., 2018) and a steady global decline in CO concentrations (Buchholz et al., 2021), demonstrate the effectiveness of targeted NTCF mitigation policies.

Numerous studies have explored the climate impacts of NTCF mitigation, with most focusing on aerosol reductions. While these yield clear air-quality benefits, they can also induce short-term warming and increases in global mean precipitation (e.g., Richardson et al., 2018; Samset et al., 2018), accompanied by a northward shift of the tropical rain belt and substantial wetting of monsoon regions (e.g., Lelieveld et al., 2019). Model simulations suggest that mid-21st-century NTCF mitigation could increase global temperature by ~0.25 K and global precipitation by ~0.3 mm day^{-1}, with aerosol reductions the dominant driver (Allen et al., 2020).

Despite this progress, most studies have examined individual NTCFs rather than their joint mitigation, and many have relied on idealised scenarios, simplified model representations of aerosol–chemistry–climate interactions, or small model ensembles, limiting the assessment of structural uncertainty. NTCFs are co-emitted from common sources and regulated through air quality policies; isolating a single species therefore misses the compound climatic response that actual mitigation measures would produce. Furthermore, previous analyses have largely focused on either global-mean temperature or precipitation or on specific regional domains, providing limited insight beyond these basic climate variables and their associated large-scale spatial patterns.

Here, we address these gaps by analysing state-of-the-art multi-model simulations from the Aerosol and Chemistry Model Intercomparison Project (AerChemMIP; Collins et al., 2017) within CMIP6 (Eyring et al., 2016). Using seven Earth System Models and a paired scenario design that isolates the NTCF signal while holding GHG forcing constant, we quantify robust near-term responses of multiple drought characteristics to NTCF mitigation across regions and seasons, and identify the large-scale dynamical mechanisms driving those responses.

https://doi.org/10.5194/egusphere-2026-3416
Preprint. Discussion started: 19 June 2026

The rest of the manuscript is organised as follows: Section 2 describes the model experiments and analysis methods. Section 3 examines the influence of NTCF mitigation on drought characteristics and the underlying mechanisms, while drought exposure is described in Section 4. Conclusions follow in Section 5.

2 Data and methods

2.1 Model data, experiments, and observations

To isolate the climate impacts of NTCFs, we analyse a pair of experiments developed along the CMIP6 Shared Socioeconomic Pathways (SSPs) projections. The baseline pathway, SSP3-7.0, is a high-emissions scenario characterised by limited international cooperation, weak air-quality regulation, and the absence of effective climate mitigation, yielding a radiative forcing of about 7.0 W m^{-2} by 2100 (Eyring et al., 2016). It represents a world with continued fossil fuel dependence and persistently high NTCF emissions, and therefore provides a reference state against which the climatic effects of NTCF mitigation can be quantified.

The companion scenario, SSP3-7.0-lowNTCF, follows the same socioeconomic pathway and GHG trajectory as SSP3-7.0, but applies stringent air-pollution controls using emission factors consistent with SSP1. The impact of NTCF mitigation is estimated as the difference between SSP3-7.0-lowNTCF and SSP3-7.0 (Allen et al., 2020), assuming approximate linear superposition of GHG and NTCF effects, a structural feature of the AerChemMIP framework shared with prior studies using the same design (Allen et al., 2020; Turnock et al., 2022). This provides an upper-bound estimate of NTCF-driven changes, as residual non-linearity, due for example to non-linear aerosol–cloud–radiation interactions, is most likely significant over regions of largest emission change, particularly South and East Asia.

We analyse seven CMIP6 Earth System Models (Table S1), each including interactive tropospheric aerosols and atmospheric chemistry and providing three ensemble members for both experiments (similarly to Allen et al., 2020). Models are analysed over 2015–2055, when air-pollution mitigation is strongest in SSP3-7.0-lowNTCF. Historical simulations are used as a baseline and to evaluate model skill against observations. Observed temperature and precipitation are taken from the CRU TS v4.02 dataset (0.5° × 0.5°; Moseid et al., 2020). Future changes are assessed by comparing 2036–2055 with 1995–2014. Population exposure to drought is quantified as the product of drought occurrence (in months) and gridded population count, aggregated over each region. Present-day population distributions are taken from the Gridded Population of the World version 4 (GPWv4; CIESIN, 2018) dataset for 2000 at 30 arc-minute resolution, regridded to the common 2.5° × 2.5° analysis grid. We use a fixed present-day population rather than scenario-projected population in order to isolate the climatic component of exposure change; the use of SSP3-projected mid-century population would amplify exposure estimates substantially, particularly over South Asia and sub-Saharan Africa where demographic growth is largest under SSP3.

https://doi.org/10.5194/egusphere-2026-3416
Preprint. Discussion started: 19 June 2026

Model responses are first averaged across ensemble members and then combined into an equally weighted multi-model ensemble (MME). All fields are bilinearly interpolated to a common 2.5° × 2.5° grid prior to analysis, and inter-model robustness is assessed from the distribution of individual-model changes and their agreement (5 out of 7). Statistical significance of the difference in MME changes between SSP3-7.0 and SSP3-7.0-lowNTCF is evaluated at each grid point using a two-tailed Student's t-test using individual model differences, with results significant at the 90% confidence level indicated on figures by stippling.

The evolution of NTCF and GHG emissions under the two scenarios has been described in detail by Allen et al. (2020), and we refer the reader to that study for global mean time series and sub-continental emission trends. Briefly, CO_2 and CH_4 emissions increase by approximately 65% and 50% respectively by 2055 relative to 2015 and are identical across both scenarios, as the AerChemMIP design holds well-mixed GHG forcing constant between experiments. Under SSP3-7.0, anthropogenic emissions of most aerosol species and gaseous precursors increase modestly (5–15% by 2055), whereas SSP3-7.0-lowNTCF applies stringent air-quality controls, yielding global emissions reductions of 40–55% across all non-methane NTCFs, with SO_2 and BC showing the largest decreases, particularly over South and East Asia. Here, rather than area-averaged sub-continental trends, we show in Fig. S1 the spatial distribution of emission changes at the model grid-point level, allowing us to link local forcing anomalies directly to the regional drought response patterns described in Section 3.

2.2 Drought index and computation of drought characteristics

We use the Standardized Precipitation Evapotranspiration Index (SPEI; Vicente-Serrano et al., 2010) in preference to the Palmer Drought Severity Index (PDSI; Wells et al., 2004), whose fixed timescale and strong memory effects limit its applicability across climates, and the Standardized Precipitation Index (SPI; McKee et al., 1993), which neglects temperature-driven evaporative demand.

SPEI combines SPI's multitemporal framework with a PDSI-like physically based water-balance approach by incorporating potential evapotranspiration (PET), allowing droughts driven by both precipitation deficits and enhanced evaporative demand to be captured (Vicente-Serrano et al., 2010). SPEI has proven effective for global and regional drought assessments under climate change and remains computationally efficient (Begueria et al., 2013). We therefore adopt SPEI as our drought indicator, and we focus primarily on the 3-month timescale (SPEI-3) to capture short-term agricultural stress, and their inter-seasonal contrasts. We will also examine SPEI-6 and SPEI-12 to assess the sensitivity to temporal aggregation as well as the implications for long-term moisture deficits relevant to hydrological and agricultural droughts.

The choice of a reference period is critical for calculating drought indices but often receives insufficient attention (Kwon and Sung, 2019; Wang et al., 2021), and can lead to substantial discrepancies in evaluating drought severity and spatial extent (Um et al. 2017). The SPEI was standardised using 1985–2014 as the reference period, providing a 30-year climatological baseline

https://doi.org/10.5194/egusphere-2026-3416
Preprint. Discussion started: 19 June 2026

for estimating the probability distribution of the climatic water balance. This reference period was used only for SPEI standardisation, and for defining drought anomalies relative to the late historical climate. Drought characteristics were then calculated over 1995–2014 for the historical baseline and over 2036–2055 for the future period, so that both periods span 20 years and are directly comparable. This choice ensures a consistent comparison between the historical period and the future period 2036–2055, while retaining a sufficiently long baseline for SPEI calculation.

Drought events are identified using the "run theory" (Yevjevich, 1969), whereby a drought event is defined as a continuous period during which monthly SPEI values remain below a prescribed threshold. The SPEI at each grid cell and timescale is standardised against the reference period climatology such that its values follow a standard normal distribution with zero mean and unit variance; a value of −1 therefore corresponds to conditions at approximately the 16th percentile of the historical water-balance distribution, indicative of moderate drought. This threshold is widely used in the literature to define moderate drought conditions (McKee et al., 1993; Lloyd-Hughes and Saunders, 2002) and provides a balance between capturing meaningful drought episodes and maintaining a sufficient sample size for robust statistical analysis. Drought occurrence is defined as the frequency of drought months, duration as the number of consecutive months below the threshold, severity as the cumulative SPEI deficit over the event, and intensity as the mean SPEI value during the event. Although drought occurrence, intensity, and severity were analysed at both annual and seasonal scales, drought duration is presented only at the annual scale. This is because the three-month seasonal window constrains the possible duration values and may truncate drought events that extend across adjacent seasons. Consequently, seasonal estimates of duration are more sensitive to the choice of the temporal window and are less directly comparable with annual estimates of drought persistence. Annual duration therefore provides a more robust measure of drought persistence by allowing drought events to be identified over a continuous 12-month period.

By definition, computation of the SPEI requires estimates of potential evapotranspiration (PET), the theoretical maximum rate at which water would be evaporated from the land surface and transpired by vegetation under conditions of unlimited water supply. We adopt the Hargreaves–Samani method (Hargreaves and Samani, 1985), which requires only maximum and minimum temperature and extra-terrestrial solar radiation, i.e., incoming solar radiation at the top of the atmosphere. This approach offers a physically more realistic representation of evaporative demand than the temperature-only Thornthwaite method while remaining computationally tractable for large multi-model ensemble analyses (De Sousa Lima et al., 2013; Ogunrinde et al., 2021).

https://doi.org/10.5194/egusphere-2026-3416
Preprint. Discussion started: 19 June 2026

3 Results

3.1 Water availability trends

To place the analysis into context, we first examine the evolution of temperature and precipitation, and the drought-relevant indicator SPEI-3 under the two scenarios, before turning to a detailed characterisation of drought characteristics in subsequent sections.

Global-mean MME SPEI-3 displays an approximately linear and statistically significant (95% confidence level) decrease throughout the entire analysis period, with a historical trend of -0.046 decade^{-1} over 1995-2014 that continues largely uninterrupted into the future under both scenarios (-0.047 decade^{-1} and -0.049 decade^{-1} in SSP3-7.0 and SSP3-7.0-lowNTCF, respectively over 2015- 2055; Fig. 1a). Starting from a near-zero baseline mean over 1995-2014, global-mean SPEI-3 reaches approximately -0.2 by mid-century, indicative of increasingly drought-prone conditions (Fig. 1a).

https://doi.org/10.5194/egusphere-2026-3416
Preprint. Discussion started: 19 June 2026

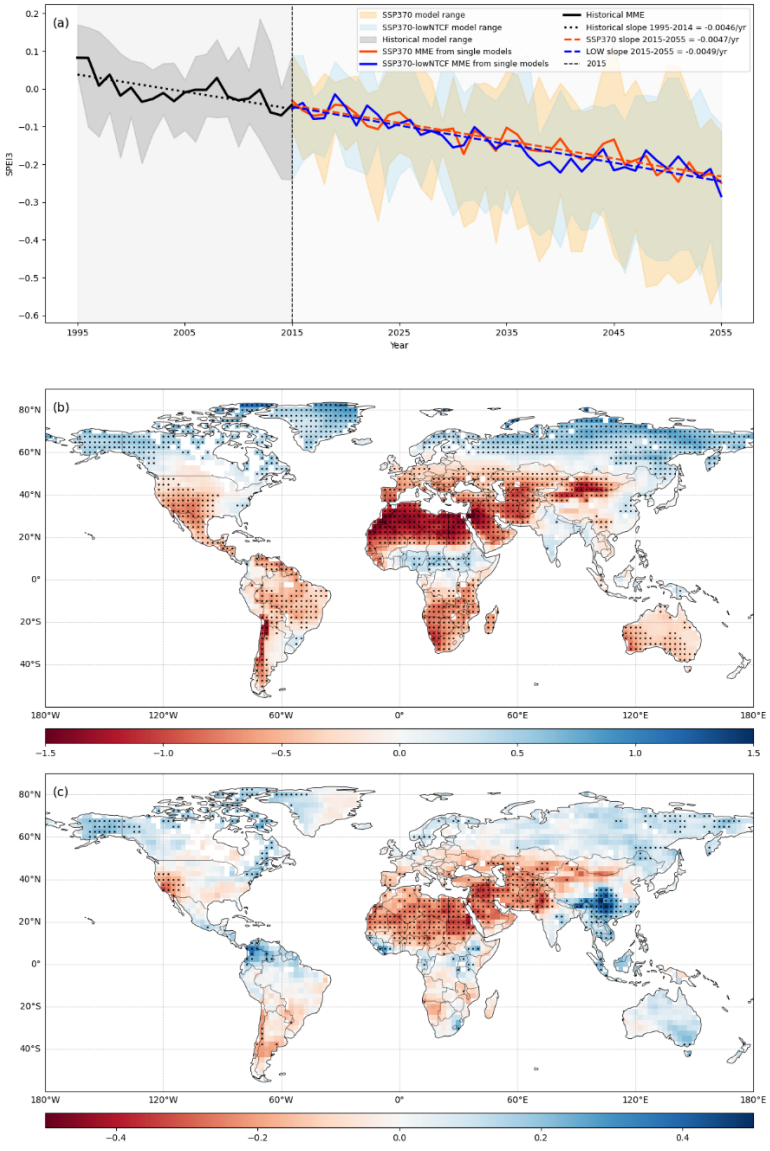

Figure 1: (a) Time series of global annual mean SPEI-3 for the historical (1995-2014) and future (2015-2055) periods. The solid lines represent the MME (historical: black; SSP3-7.0: red; SSP3-7.0-lowNTCF: blue), while the shading represents the inter-model range. The dotted and dashed lines are the least-square linear fits to the historical and future time series. (b) Spatial pattern of changes in MME SPEI-3 under SSP3-7.0 during 2036-2055 relative to 1995-2014. (c) Changes in MME SPEI-3 during 2036-2055 due to NTCF mitigation (difference between SSP3-7.0-lowNTCF – SSP3-7.0). Black dots in (b) and (c) indicate grid cells where changes are statistically significant at the 95% level based on the two-tailed Student's t-test.

This drying signal is robust and statistically significant across models, though with substantial inter-model spread in the magnitude of the signal (ranging from -0.01/-0.01 to -0.11/-0.09 decade^{-1} across the seven models for SSP3-7.0/SSP3-7.0-

https://doi.org/10.5194/egusphere-2026-3416
Preprint. Discussion started: 19 June 2026

lowNTCF), and reflects the dominant influence of rising evaporative demand associated with global warming, which outweighs the concurrent increase in global-mean precipitation. Differences between SSP3-7.0 and SSP3-7.0-lowNTCF are negligible and statistically insignificant in the global mean, with the latter showing only a marginally more negative trend. This indicates that NTCF mitigation exerts little influence on global-mean drought tendency, a consequence of strong regional heterogeneity and partial compensation between temperature- and precipitation-driven contributions to SPEI, particularly between the drying signal over the subtropics and the mid-latitudes, and the wetting signal over monsoon regions and high northern latitudes. However, global-scale metrics can obscure important spatial structure in the drought response, and studies focused solely on global or hemispheric means may substantially underestimate, or entirely miss, the regional drought hazards that NTCF mitigation can both alleviate and exacerbate (Seneviratne et al., 2012).

The spatial patterns of the SSP3-7.0 2036-2055 annual mean SPEI-3 changes compared to the historical (1995-2014) period reveal coherent large-scale structures (Fig. 1b). Under SSP3-7.0, widespread drying emerges across tropical and mid-latitude regions in both hemispheres, with the strongest decreases over arid and semi-arid regions (northern Africa, the Mediterranean, the Middle East, central Asia, and southern Africa). These are regions characterised by low baseline precipitation and high evaporative demand, and thus are particularly sensitive to further warming. The projected SPEI-3 decreases in regions such as northern Africa, the Middle East, and central Asia, the future SPEI-3 anomaly reach −1 to −1.5 standard deviations of the detrended historical SPEI-3 distribution. This implies that future mean SPEI-3 conditions in these regions will fall below what has recently been experienced during drought years, representing a shift toward unprecedented aridity within the 2036–2055 timeframe. In contrast, wetter conditions develop over equatorial Africa, South and East Asia, the eastern United States, and high northern latitudes.

For reference, the historical mean SPEI-3 (Fig. S2) confirms that much of the projected future drying under SSP3-7.0 occurs over regions already exhibiting negative SPEI anomalies during 1995–2014, representing a substantial amplification of already-emerging tendencies. However, central Europe, the central US, South Africa, and parts of tropical South America show near-neutral historical SPEI-3 values yet project strong future drying, suggesting a qualitative shift in their hydroclimate rather than simple intensification.

An overall similar structure is also displayed under SSP3-7.0-lowNTCF, attesting to the predominant role of GHG increases in shaping the large-scale response (Fig. 1c). However, the magnitude of regional anomalies is substantially modulated by NTCF mitigation, with the signal robust across the majority of models over the majority of the areas. Drying is amplified over northern Africa, the Middle East, Europe, and the western United States, where precipitation decreases are accompanied by marked warming and enhanced evaporation. Conversely, wetter conditions intensify over South and East Asia, the Amazon, Central America, and much of Australia. A pronounced zonal dipole emerges over Eurasia, with enhanced water scarcity over already relatively dry western regions and substantially reduced drought-favourable conditions over monsoon-dominated

https://doi.org/10.5194/egusphere-2026-3416
Preprint. Discussion started: 19 June 2026

eastern Asia, consistent with aerosol reductions driving a stronger Asian monsoon (Wilcox et al., 2020; Allen et al., 2020). Exceptions where NTCF mitigation reverses the GHG-driven drying signal — including parts of Central America, the Amazon, southern Africa, and Australia — are associated with significant regional wetting that offsets the evaporative demand increase; a more detailed attribution of these reversals, including the role of circulation changes, is provided in Section 3.3.

These SPEI-3 responses reflect the underlying changes in effective radiative forcing, temperature, and precipitation induced by NTCF mitigation, which are spatially heterogeneous and consistent with Allen et al. (2020) and Turnock et al. (2022). The specific dynamical and thermodynamic mechanisms are examined in Section 3.3.

3.2 NTCF mitigation and changes in drought characteristics

This section examines the projected seasonal changes in drought characteristics due to NTCF mitigation. The spatial patterns of the three metrics — occurrence, duration, and intensity — are generally consistent; we therefore focus on drought occurrence in the main figures, while changes in duration and intensity are shown in the supplementary material. We focus primarily on DJF and JJA to highlight the contrasting impacts of NTCF mitigation between the two peak seasons of the annual cycle; corresponding patterns for MAM and SON are also shown in the supplementary material and referred to where relevant.

Under SSP3-7.0, drought occurrence increases substantially relative to the historical period across all seasons (Figs. 2a and 2c).

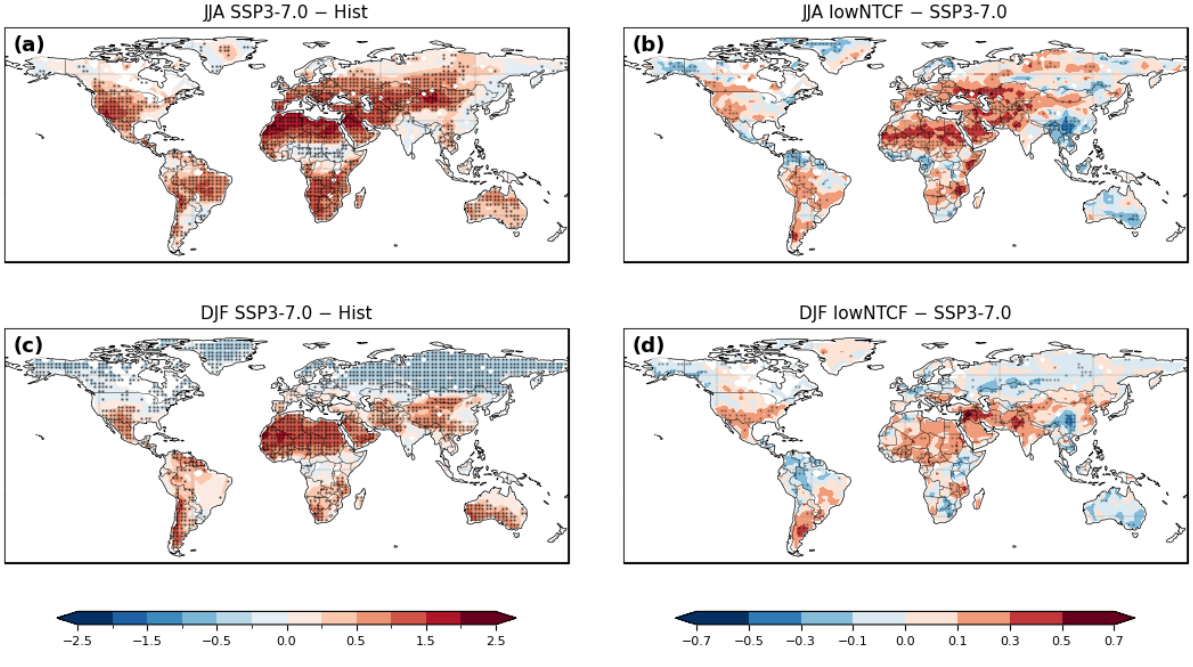

https://doi.org/10.5194/egusphere-2026-3416
Preprint. Discussion started: 19 June 2026

Figure 2: (a) and (c): Spatial patterns of MME changes in drought occurrence (months season^{-1}) under SSP3-7.0 during 2036-2055 relative to 1995-2014 for (a) JJA and (c) DJF. (b) and (d): MME changes in future drought occurrence during 2036-2055 due to NTCF mitigation for (b) JJA and (d) DJF. Stippling marks grid cells where the difference is statistically significant at the 90% level using a two-tailed Student's t-test.

During JJA, widespread increases are projected across the Northern Hemisphere, affecting western and central America, Europe, northern Africa, the Middle East, and central Asia. The largest anomalies, exceeding 2 months per season, are concentrated over northern Africa and parts of the Middle East — regions where drought occurrence is already elevated in the historical climatology (Fig. S3), underscoring that NTCF-driven warming is superimposed on already drought-prone backgrounds. Large increases are also seen in the Southern Hemisphere, particularly over southern Africa and the Amazon, exacerbating water scarcity during the climatological dry season. During DJF, increases over northern Africa, the Middle East, and the western US persist but are generally of smaller magnitude than in JJA. Positive anomalies also extend over Pakistan, northwestern India, and central China. The SON pattern closely resembles JJA, with the largest Southern Hemisphere increases occurring in that season, while MAM closely mirrors DJF, with peak anomalies over the western US and parts of Asia (Fig. S4). The timing of peak drought occurrence broadly follows the seasonal cycle of maximum temperature and evaporative demand in each region, consistent with the thermodynamic control on the water balance. However, a close examination reveals some important differences in the timing of the peak values. For example, the largest increases across the southern hemisphere are found in SON, while the largest magnitude is in JJA over the US and Europe.

NTCF mitigation (Figs. 2b and 2d) yields a predominantly positive response in drought occurrence — that is, reducing NTCFs generally increases drought frequency beyond what is projected under SSP3-7.0 alone. During JJA, the largest and most statistically significant increases under NTCF mitigation are found over northern Africa and the Middle East (exceeding 0.5 months per season in the multi-model mean), Europe, western America, and parts of southern Africa and South America. In the majority of these regions, the NTCF mitigation signal amplifies drought anomalies that are already positive under SSP3-7.0, effectively compounding the GHG-driven drying. For example, over the Sahara and West Asia, NTCF mitigation adds approximately 0.3–0.5 months per season of additional drought occurrence on top of increases of 1.5–2 months per season already present under SSP3-7.0. During DJF, the pattern of increases under NTCF mitigation shifts somewhat southward and eastward, with notable increases over South Asia, the eastern Mediterranean, and the Middle East. Reductions in drought occurrence under NTCF mitigation — indicating a beneficial effect — are confined to limited areas, primarily southeastern Asia, eastern Australia, and parts of Central America, consistent with the precipitation increases in those regions. The signal is robust across models, with at least 5 out of 7 models agreeing on the sign of the change over the main hotspot regions (stippling in Fig. 2). Compared to SSP3-7.0, the timing of peak increases under NTCF mitigation is broadly similar, although the DJF signal shows a more marked response concentrated over South and Central Asia relative to the JJA pattern, reflecting the seasonal modulation of the large-scale circulation response discussed in Section 3.3.

https://doi.org/10.5194/egusphere-2026-3416
Preprint. Discussion started: 19 June 2026

In most regions, drought events under NTCF mitigation tend to cluster in the same seasons where occurrence is already elevated under SSP3-7.0 relative to the historical baseline, thus further compounding an already increased drought hazard. The seasonal timing of peak drought occurrence is broadly preserved between the two scenarios across most regions, with both SSP3-7.0 and SSP3-7.0-lowNTCF showing maximum values during JJA and SON, and comparatively modest changes during DJF and MAM. In some areas, however, the largest enhancement due to NTCF mitigation is not during the season of peak drought occurrence in SSP3-7.0, such as prominently over the Mediterranean and central Europe, where the strongest increases in drought occurrence emerge in SON rather than in summer, reflecting a seasonally asymmetric response driven by circulation changes and moisture availability. Another notable exception is the Amazon region where NTCF mitigation produces a reduction in drought occurrence relative to SSP3-7.0 during DJF and MAM, while an opposite response—an increase in drought occurrence—emerges during SON.

Changes in drought intensity and duration under NTCF mitigation are broadly spatially consistent with the occurrence signal (Figs. S5, S6). Intensity increases — indicating more negative mean SPEI during drought events — are concentrated across the Middle East, Central Asia, and northern Africa, with the strongest and most model-robust signal in JJA and SON; the Mediterranean also shows notable increases in those seasons. Annual drought duration increases are most coherent across Central Asia and the Middle East, where anomalies exceed 0.5 months per event, with more modest but significant increases across the Sahel and parts of western North America. Modest reductions in both metrics are found over Southeast Asia, Central America, and central Africa, consistent with the wetting response in those regions. Broadly, the three metrics are approximately aligned, suggesting that NTCF mitigation drives a compound intensification of drought — simultaneously more frequent, longer-lasting, and more severe — across much of the Northern Hemisphere dryland belt, particularly in seasons and regions where GHG-driven drying is already most pronounced.

3.3 Mechanisms underpinning changes in droughts

Identifying the physical mechanisms underpinning the drought changes described above is essential for building confidence in the projected responses to NTCF mitigation. To this end, we examine changes in key dynamical and thermodynamic variables, which collectively establish a physically coherent framework for interpreting future drought changes. Previous studies have shown that changes in seasonal mean environmental conditions — rather than changes in variability — are the primary driver of shifts in climate extremes (Christidis et al., 2015; Diffenbaugh et al., 2017; Seneviratne et al., 2012), as they represent the large-scale background state on top of which individual drought events develop. We note, however, that temporal changes in the intra-seasonal distribution of precipitation, even in the absence of mean changes, can also modulate drought frequency; this possibility is not explored here but warrants future investigation.

https://doi.org/10.5194/egusphere-2026-3416
Preprint. Discussion started: 19 June 2026

The spatial pattern of changes in drought occurrence bears a marked resemblance to the seasonal anomalies in precipitation (P) minus potential evapotranspiration (PET) (Fig. 3), which is physically consistent given that P − PET represents the surface water balance and serves as the direct input to the SPEI.

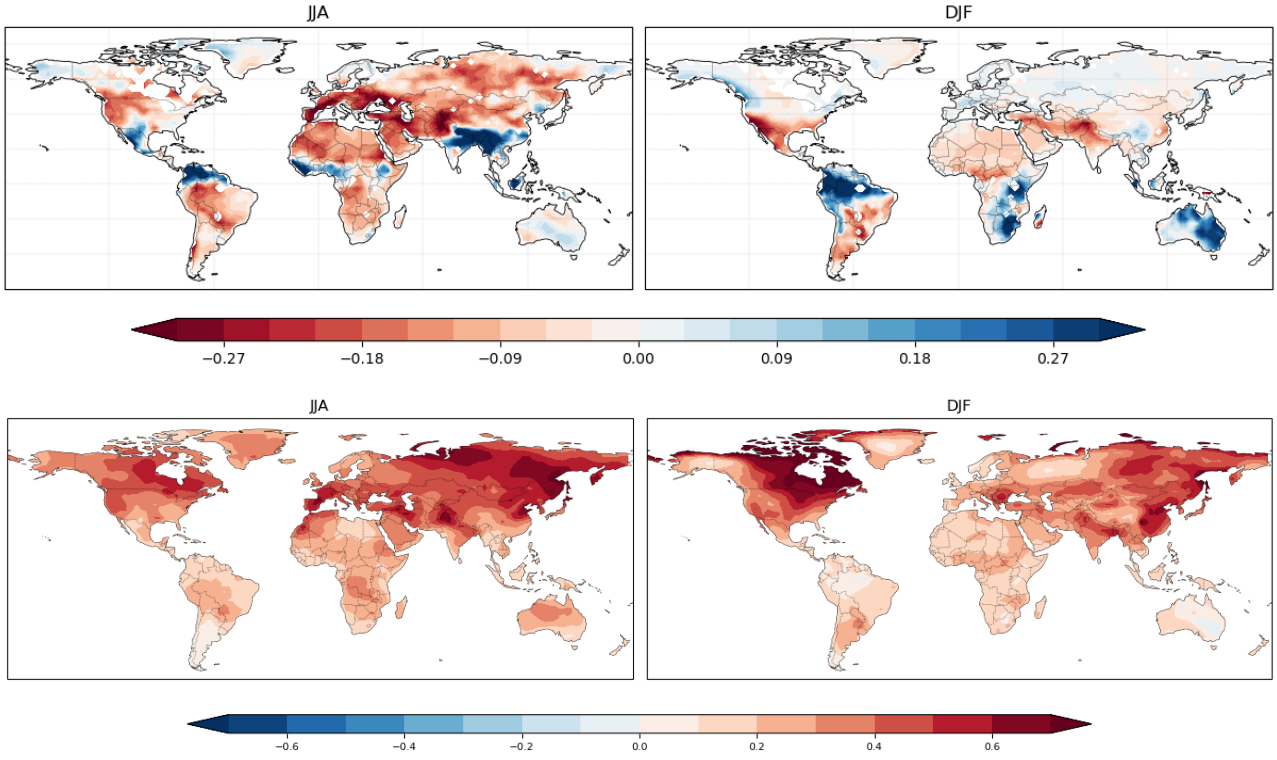

Figure 3: (Top): Spatial patterns of MME changes in precipitation minus potential evapotranspiration (P − PET) [mm day^{-1}] for (left) JJA and (right) DJF due to NTCF mitigation. (Bottom): As (Top) but for near-surface mean temperature (ΔTmean = (Tmax + Tmin)/2) [K].

Regions of increased drought occurrence broadly correspond to negative P−PET anomalies, and vice versa. Note however, that the relative magnitudes do not necessarily map straightforwardly onto one another, as the translation from a given P−PET anomaly into a change in drought occurrence depends on the underlying climatological mean and variability (e.g., a modest negative P−PET anomaly in an already arid region may drive proportionally larger shifts in drought occurrence than a comparable anomaly in a wetter climatological setting).

The relative contributions of P and PET to the P−PET anomaly are regionally distinct. In some areas, negative P−PET anomalies are dominated by precipitation suppression — for example over the southern US and Mexico in DJF, and parts of South America during JJA, where precipitation reductions are not compensated by changes in evaporative demand. In many

https://doi.org/10.5194/egusphere-2026-3416
Preprint. Discussion started: 19 June 2026

regions, however, PET increases play a dominant role, particularly across the Northern Hemisphere midlatitudes during JJA (where PET accounts for ~64% of the extratropical Δ(P−PET) signal) and over northern Africa and the Middle East, where warming-driven increases in evaporative demand suppress moisture availability even where precipitation is not substantially reduced (Fig. S7). In some areas, changes in P and PET oppose each other: over the western US during JJA, enhanced PET partially offsets concurrent precipitation increases, resulting in a net drying tendency (Fig. S7, S8). Conversely, over South and East Asia and the equatorial regions during JJA, reductions in drought occurrence are mainly driven by substantial increases in precipitation (Fig. S7), with PET changes playing a secondary role. During DJF, precipitation is the slightly dominant contributor globally (~57% of Δ(P−PET)), though over the extra-tropics P and PET contributions are roughly balanced, and the two drivers can again act in opposition. During JJA, PET becomes the dominant driver globally, with its role particularly pronounced across the Northern Hemisphere midlatitudes and the extra-tropics (~64%).

During MAM, negative P−PET anomalies are largely driven by increases in PET, particularly across the Northern Hemisphere tropical and midlatitude regions, with precipitation changes playing a secondary role (Fig. S7, S9). During SON, drying in parts of the Southern Hemisphere tropics arises from sustained PET increases, while PET anomalies continue to dominate Northern Hemisphere drying, only partly offset by concurrent precipitation increases over some regions such as North America (Fig. S7, S8, S9).

The increase in PET across the Northern Hemisphere midlatitudes is closely associated with marked near-surface warming in all seasons (Figs. 3 and S10), particularly during the daytime as indicated by the increases in the diurnal temperature range (Fig. S11). In particular, this warming plays a crucial role in driving PET increases over the western US and, even more markedly, across Eurasia. Yet, changes in NTCF emissions, already relatively low over the Northern Hemisphere extra-tropics, are relatively minor, and as such this continental warming cannot be attributed primarily to regional emission unmasking. By contrast, the largest emission changes occur over Asia. This points to the potential role of large-scale dynamical adjustments in communicating the NTCF forcing signal to remote regions. In the following paragraph, we investigate this mechanism, focusing on JJA and DJF as the two seasons that most clearly capture the contrasting atmospheric responses.

Examining first the boreal summer circulation anomalies related to NTCFs, the 300-hPa meridional wind (Fig. S12) and stream-function fields reveal a pronounced pattern of alternating positive and negative anomalies across the Northern Hemisphere midlatitudes (Fig. 4, top), consistent with a quasi-stationary Rossby wave train. The wave activity flux (WAF) provides independent support for this interpretation, as it is parallel to the wave group velocity and thus traces the propagation pathway.

https://doi.org/10.5194/egusphere-2026-3416
Preprint. Discussion started: 19 June 2026

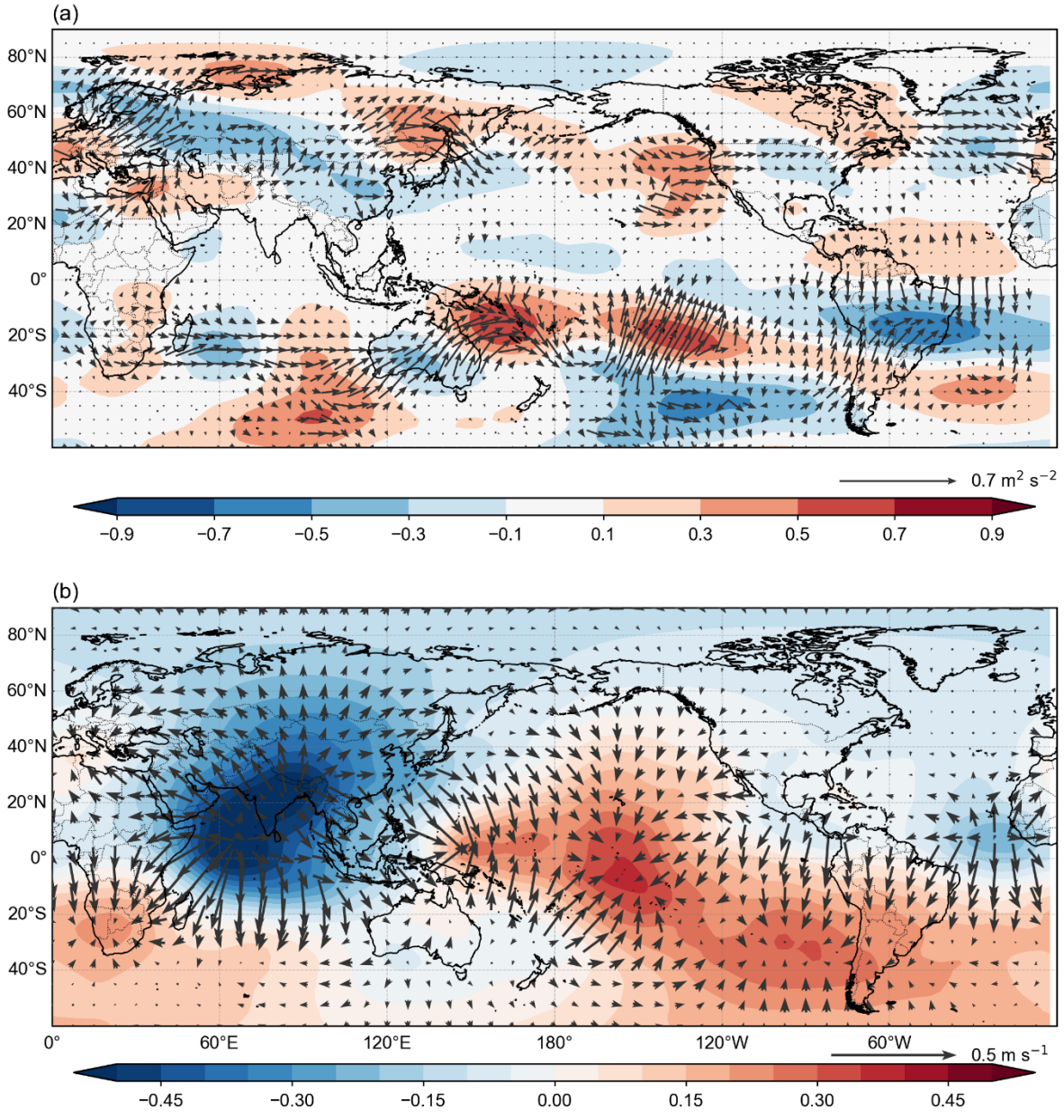

Figure 4: (a): Spatial pattern of JJA changes during (2036-2055) in 300-hPa stream function (unit: 10^6 m^2 s^{-1}; shading) and wave activity flux (unit: 10 m^2 s^{-2}; vectors) due to NTCF mitigation. (b): As (a) but for 150-hPa velocity potential (unit: 10^6 $m^2 s^{-1}$; shading) and divergent wind (unit: m s^{-1}; vectors).

https://doi.org/10.5194/egusphere-2026-3416
Preprint. Discussion started: 19 June 2026

A strong WAF anomaly emanates from northern India and central China, indicating a source of wave activity, and propagates north-eastward toward the north-western Pacific, before turning eastward across North America, the north Atlantic, and into Europe and the Middle East, where it progressively weakens. The origin of this teleconnection is clarified by the Rossby wave source (RWS) diagnostic. A marked RWS dipole coincides with the anomalous convection over South and East Asia (Fig. S13), where strong upper-level divergent outflow associated with the enhanced precipitation anomaly interacts with the large meridional vorticity gradient of the Asian–Pacific jet, generating the primary source of tropical Rossby wave activity. Secondary RWS anomalies are also present over the extratropical north-western Pacific, the north Atlantic, and north-eastern Europe, collocated with the climatological jet exit regions — well-known nodal points for midlatitude wave–mean flow interaction. These can be interpreted as secondary sources arising from the quasi-geostrophic adjustment of the large-scale flow to the wave generated in the primary source region. An analogous wave train in the Southern Hemisphere originates from upper-tropospheric divergence over the Indian Ocean, propagates downstream toward Australia, and progressively weakens as it approaches South America.

Mid-tropospheric descent is dynamically linked to upper-tropospheric southward wind anomalies on the eastern flanks of anomalous upper-level anticyclones. For example, a surface anticyclonic anomaly and widespread mid-tropospheric subsidence (Fig. S14, S15) is present over Southern Europe and the Mediterranean, which amplifies surface heating through two pathways: reduced cloud cover enhances downwelling shortwave radiation at the surface, and adiabatic warming of descending air increases near-surface temperatures. Conversely, in the southern Hemisphere, an anomalous upper-level cyclonic circulation over western and central Australia is associated with anomalous ascent, contributing to the modest wetting and associated reduction in drought occurrence in that region.

In addition to exciting midlatitude Rossby wave responses, the convective anomaly over Asia also drives marked adjustments in the tropical zonal overturning circulation, as shown by the anomalous upper-tropospheric velocity potential and divergent wind (Fig. 4, bottom). The dominant feature is strong upper-level outflow centred over South Asia, associated with the enhanced monsoonal precipitation. One branch of this outflow heads north-westward, converging and subsiding over the Middle East, northern Africa, and the southern Mediterranean, a response reminiscent of the monsoon-desert mechanism (Rodwell and Hoskins, 1996; Cherchi et al., 2016), whereby enhanced monsoon heating drives compensating subsidence over adjacent arid regions. A second branch is directed south-westward, inducing convergence and mid-tropospheric subsidence over southern Africa. In both cases, the remotely forced descent suppresses precipitation, enhances surface warming and evapotranspiration, and thereby increases drought occurrence. Further to the west, anomalous wetting over the north equatorial Atlantic, associated with a narrowing and intensification of the regional ITCZ linked to the subsidence anomalies described above, drives upper-tropospheric divergent flow toward the Amazon basin, generating anomalous descent and drying in that region.

https://doi.org/10.5194/egusphere-2026-3416
Preprint. Discussion started: 19 June 2026

The DJF teleconnection pattern (Fig. 5) shares structural similarities with JJA but is characterised by a distinct source region and propagation pathway.

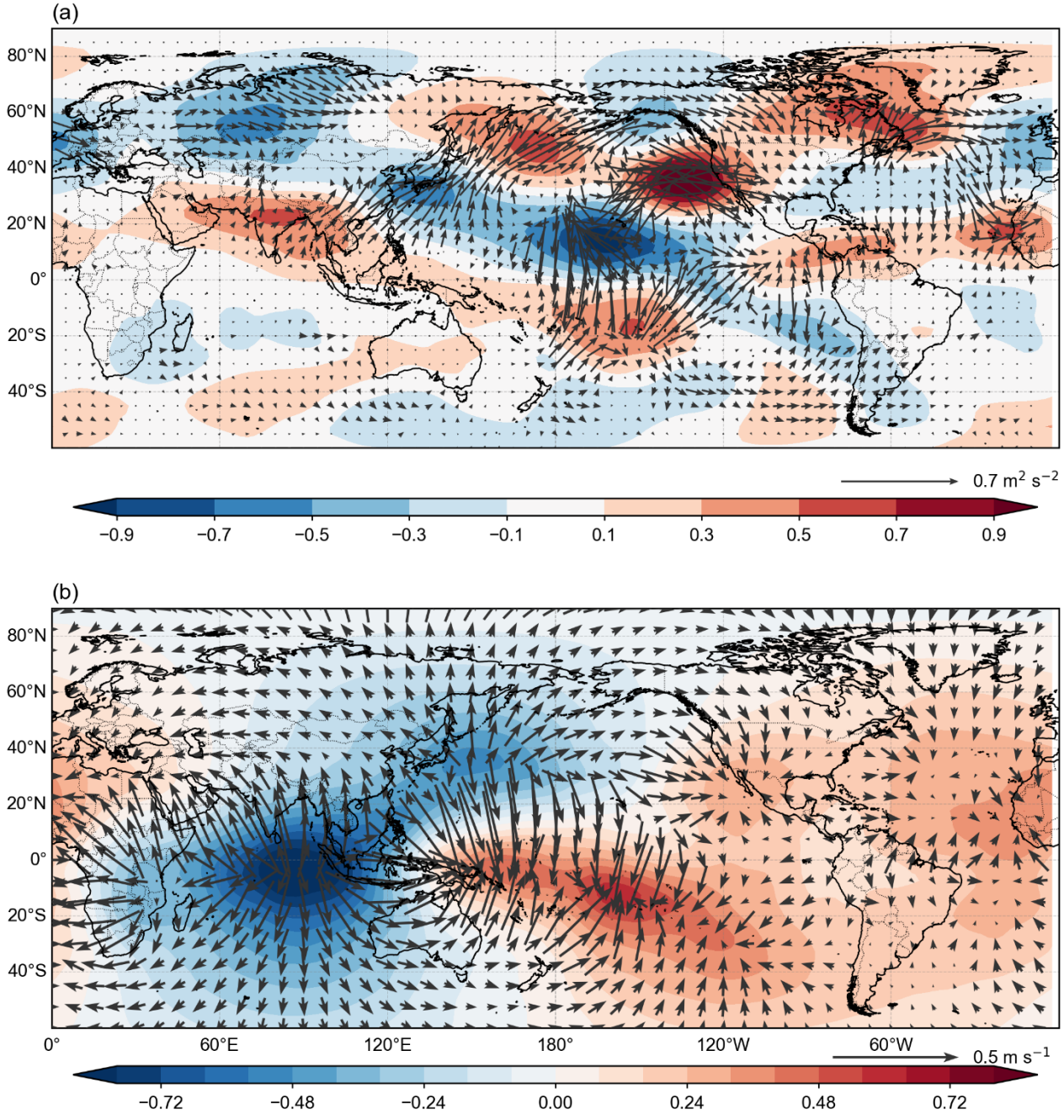

Figure 5: As Figure 4, but for DJF.

https://doi.org/10.5194/egusphere-2026-3416
Preprint. Discussion started: 19 June 2026

A marked positive precipitation anomaly extends from the central equatorial Indian Ocean to the Maritime Continent, while the western equatorial Pacific and the South Pacific Convergence Zone (SPCZ) experience drying, consistent with a westward shift of the Pacific Walker circulation. Enhanced precipitation also occurs across south-eastern and eastern Asia, accompanied by a weakening of the Siberian High and reduced northerly flow over East Asia, consistent with the well-documented sensitivity of the East Asian winter monsoon to aerosol forcing (Liu et al., 2018). One branch of the associated upper-tropospheric divergent flow heads north-westward, generating widespread subsidence across central and northern Africa, the Middle East, and southwestern Asia. Another branch propagates northward into the midlatitude westerlies, exciting an eastward-propagating Rossby wave train broadly analogous to its JJA counterpart, with alternating cyclonic and anticyclonic anomalies crossing North America and the north Atlantic before reaching Europe. The anomalous descent over western North America drives land drying and warming over northern Mexico and the southwestern US. In contrast to JJA, the DJF wave response in the Southern Hemisphere is negligible, owing to the weaker seasonal baroclinicity of the Southern Hemisphere during austral summer.

3.4 Variations of drought characteristics at different time scales

Examining drought responses across multiple timescales is important because SPEI-3 primarily reflects short-term meteorological drought, SPEI-6 is more indicative of agricultural drought, and SPEI-12 captures hydrological drought relevant to long-term water resource management (McKee et al., 1993; Vicente-Serrano et al., 2010). Fig. 6 compares the influence of NTCF mitigation on annual drought occurrence at the three timescales, and the corresponding patterns for duration and intensity are provided in Figs. S6 and S16, respectively.

https://doi.org/10.5194/egusphere-2026-3416
Preprint. Discussion started: 19 June 2026

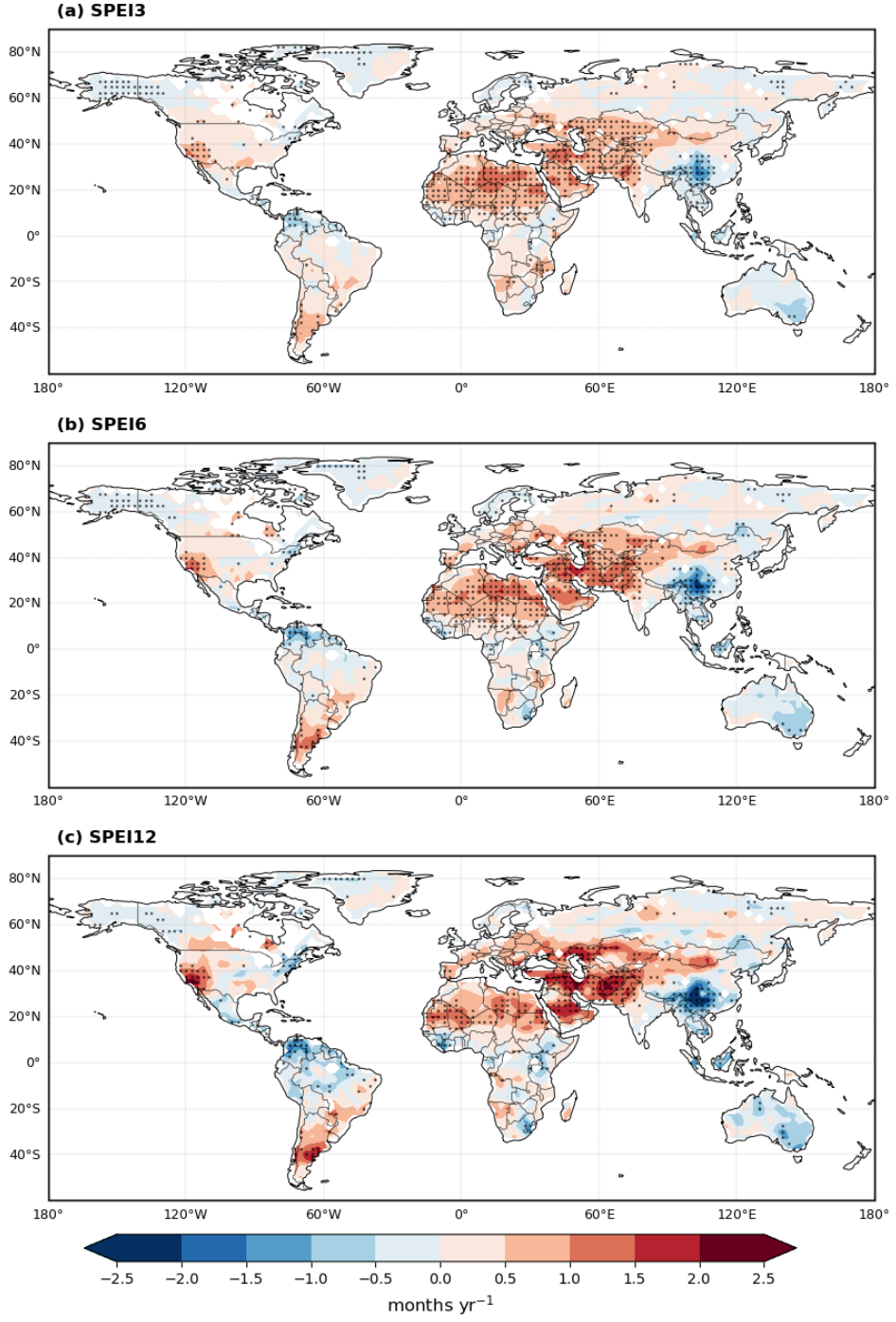

Figure 6: Spatial patterns of MME changes in annual drought occurrence (months year^{-1}) due to NTCF mitigation during 2036-2055 for (a) SPEI-3, (b) SPEI-6, and (c) SPEI-12. Stippling marks grid cells where the difference is statistically significant at the 90% level using a two-tailed Student's t-test.

https://doi.org/10.5194/egusphere-2026-3416
Preprint. Discussion started: 19 June 2026

Across all three timescales, the drought occurrence response patterns share a common geographic footprint, with the largest and most extensive increases concentrated over northern Africa, the Middle East and central Asia, parts of Europe, and the western US, all located predominantly in the Northern Hemisphere. Weaker and less spatially consistent increases are also found over southern Argentina and southwestern Africa at short timescales. Decreases are generally modest and spatially limited, occurring mainly over southern China, southeastern Australia, and parts of Central and northern South America. Changes in duration and intensity show a broadly similar regional structure, including marked increases over the region encompassing northern Africa, the Mediterranean, the Middle East and central Asia, and positive anomalies over the southwestern US. Decreases in all three characteristics are consistently found over southeastern China, tropical America, and southeastern Australia. This cross-timescale coherence reflects the common physical pathway by which NTCF mitigation reshapes the large-scale distribution of precipitation and evaporation, creating a geographically consistent predisposition for drought change.

Despite this overall consistency, systematic differences emerge as the accumulation period lengthens. Drought occurrence increases become progressively more spatially concentrated with increasing timescale, with anomalies focusing on the main hotspots, particularly the Middle East and central Asia, the western US, and southern Europe, while changes in surrounding regions diminish toward negligible values. Concurrently, the magnitude of anomalies over these hotspots intensifies. Similar behaviour applies to drought duration and, to a lesser extent, intensity. One notable exception occurs over some areas of northern Africa, where SPEI-6 and SPEI-12 patterns show an apparent decrease in drought duration accompanied by a compensating increase in occurrence: as the number of drought events become sufficiently large, the finite sample size leads to more frequent but shorter events being identified, so that occurrence and duration changes partially offset each other. Sub-regional differences across timescales can also lead to sign reversals. For example, NTCF mitigation produces a weak increase in drought occurrence and duration over Mexico and parts of northern South America at the 3-month timescale, transitioning to a weak decrease at SPEI-6 and a more pronounced reduction at SPEI-12. A similar reversal is seen over southern Africa, reflecting the growing influence of seasonal precipitation increases at longer integration windows. Also, noteworthy is the non-linearity in drought occurrence and duration with the increased timescale that is visible in several regions, such as the Middle East and central Asia as well as Europe and the western US, whereby occurrence rapidly increases from SPEI-6 to SPEI-12.

Drought intensity shows less variation across timescales than frequency or duration, except over parts of northern Africa and the Middle East. This is because intensity is primarily governed by short-term extremes in the water balance (P−PET): achieving a strongly negative SPEI-12 value requires either an exceptionally severe single dry season or a prolonged succession of moderate deficits, both of which are relatively rare and geographically confined. By contrast, SPEI-3 responds rapidly to short seasonal deficits, making it more sensitive to month-to-month variability. Accordingly, monthly-scale drying can produce

https://doi.org/10.5194/egusphere-2026-3416
Preprint. Discussion started: 19 June 2026

pronounced SPEI-3 anomalies that are substantially damped in SPEI-12. In arid and semi-arid regions, where PET dominates the water balance and evaporative demand amplifies under warming, longer timescales tend to reinforce and accumulate the effects of repeated short-term deficits, leading to progressively larger SPEI-12 anomalies. In more humid regions, by contrast, short droughts manifest clearly in SPEI-3 but are dampened in SPEI-12 by the buffering effect of residual soil moisture and groundwater storage.

In summary, the cross-timescale coherence of the drought response, combined with its progressive concentration and intensification at longer accumulation periods, implies that NTCF mitigation carries differentiated implications for agricultural drought risk (most visible at SPEI-3 and SPEI-6) and longer-term hydrological stress (most clearly captured by SPEI-12).

3.5 Changes in drought-affected area

Figure 7 presents the seasonal drought-affected area based on SPEI-3 for JJA and DJF, distinguishing grid cells that are drought-affected under both scenarios (grey), only under SSP3-7.0-lowNTCF (red), or only under SSP3-7.0 (blue), with robustness defined as agreement among at least five of seven models. Corresponding patterns for MAM and SON are shown in Fig. S17.

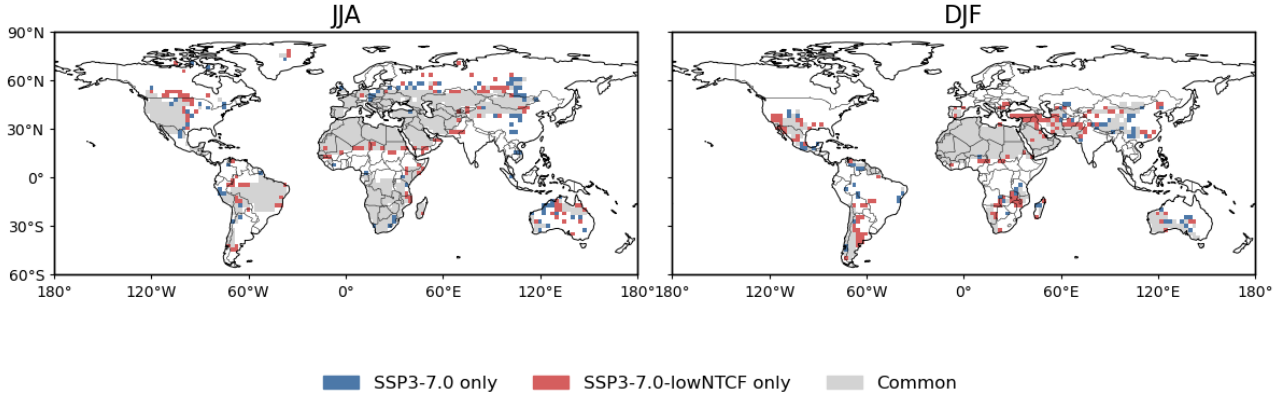

Figure 7: MME changes in seasonal drought area during 2036–2055 for (left) JJA and (right) DJF based on SPEI-3. A grid cell is defined as a drought area when at least two months within the season have SPEI ≤ −1 for at least five years during 2036–2055. Drought areas are shown only where at least five out of seven models agree on the sign. Blue indicates areas where drought occurs only under SSP3-7.0, red indicates areas where drought occurs only under SSP3-7.0-lowNTCF, and grey indicates areas common to both scenarios.

https://doi.org/10.5194/egusphere-2026-3416
Preprint. Discussion started: 19 June 2026

In JJA (and SON), the grey shading dominates the map, covering large contiguous areas across northern Africa, the Sahel, the Middle East, central Asia, South Asia, and parts of southern Europe and North America. This pervasive common signal reflects the strength of GHG-forced drying in the boreal spring and summer seasons, which is sufficiently robust across models to emerge regardless of NTCF policy. The implication is striking: across much of the Northern Hemisphere's most drought-vulnerable regions, the trajectory toward persistent drought is largely locked in by greenhouse gas forcing and related warming, and NTCF mitigation does not substantially alter it. In DJF, the grey shading contracts markedly and becomes more spatially fragmented, confined mainly to northern Africa, the Middle East, and central Asia, indicating that the common GHG-forced drought signal is weaker and less spatially extensive in the boreal winter. In MAM, the grey signal is somewhat similar to DJF, with coherent common drought areas still present across the Middle East, northern Africa, and Central Asia, but with noticeably more coverage over South Asia and southern Europe compared to DJF. SON broadly resembles JJA in the geographic distribution of grey shading, with the spatial extent somewhat more extensive particularly over North and South America and Australia, suggesting a degree of seasonality in the persistence of the GHG-forced signal even within the warm half of the year. Overall, this finding underscores the primacy of CO_2 mitigation for drought risk reduction at the global scale.

Red grid cells, where model-robust drought occurs exclusively under SSP3-7.0-lowNTCF, exceed blue ones in spatial extent across all seasons, confirming that the net effect of NTCF mitigation is to expand rather than contract the robustly drought-affected area. In JJA, red shading appears at the margins of the grey-dominated zones, particularly over parts of north America, northern Africa, scattered areas across South Asia and Australia. In DJF, red areas are more spatially distinct from the grey core, appearing over parts of the Middle East and South Asia, the Mediterranean, and portions of South America. In MAM, red shading is notably concentrated over the Middle East and parts of Central Asia, broadly consistent with the DJF pattern, though with additional red cells appearing over South Asia (a region that shows relatively limited signal in the other seasons). SON shares much of this geography but also shows scattered red cells over parts of northern Eurasia and Canada. Blue shading, indicating regions where robust drought is suppressed under reduced NTCF emissions, is considerably more limited across all seasons. The clearest blue signal appears over East Asia, consistent with the strengthened monsoon precipitation discussed in Section 3.3, while everywhere else the blue shading is sparse and geographically fragmented.

Across all four seasons, several regions emerge where red shading is present in three or more seasons, implying that NTCF mitigation drives a robust expansion of drought area that is not confined to a single season but instead represents a near-persistent shift in drought hazard. The Middle East and parts of Central Asia stand out most clearly in this regard, with red cells appearing consistently across DJF, MAM, and JJA, and to a lesser degree in SON. Central Africa and the western/central US similarly show red shading across multiple seasons. By contrast, blue cells rarely recur across more than one season in the same location, reinforcing the asymmetry of the NTCF mitigation effect: where drought relief occurs, it tends to be seasonally confined, while drought expansion under SSP3-7.0-lowNTCF is more persistent through the year.

https://doi.org/10.5194/egusphere-2026-3416
Preprint. Discussion started: 19 June 2026

The seasonal contrast between JJA and DJF is therefore striking: in JJA the response is dominated by a large common GHG-forced drought area with NTCF mitigation playing a secondary modulating role at its margins, while in DJF the scenario-dependent signals become relatively more prominent against a weaker common background. MAM and SON occupy intermediate positions, sharing the large grey-dominated structure of JJA while exhibiting some of the more distinct red-cell geography characteristic of DJF. Across all seasons, where NTCF mitigation does produce a distinct robust signal across models, it manifests overwhelmingly as drought expansion rather than relief, with the Middle East, Central Asia, northern Africa, the Mediterranean and the southwestern US emerging as the regions of greatest and most seasonally persistent concern.

3.6 Drought changes across regions and seasons

Figure 8 summarises projected changes in drought occurrence, duration, intensity, and severity across IPCC AR6 reference regions for 2036–2055 (SSP3-7.0-lowNTCF − SSP3-7.0), based on SPEI-3, allowing direct cross-regional and cross-seasonal comparison.

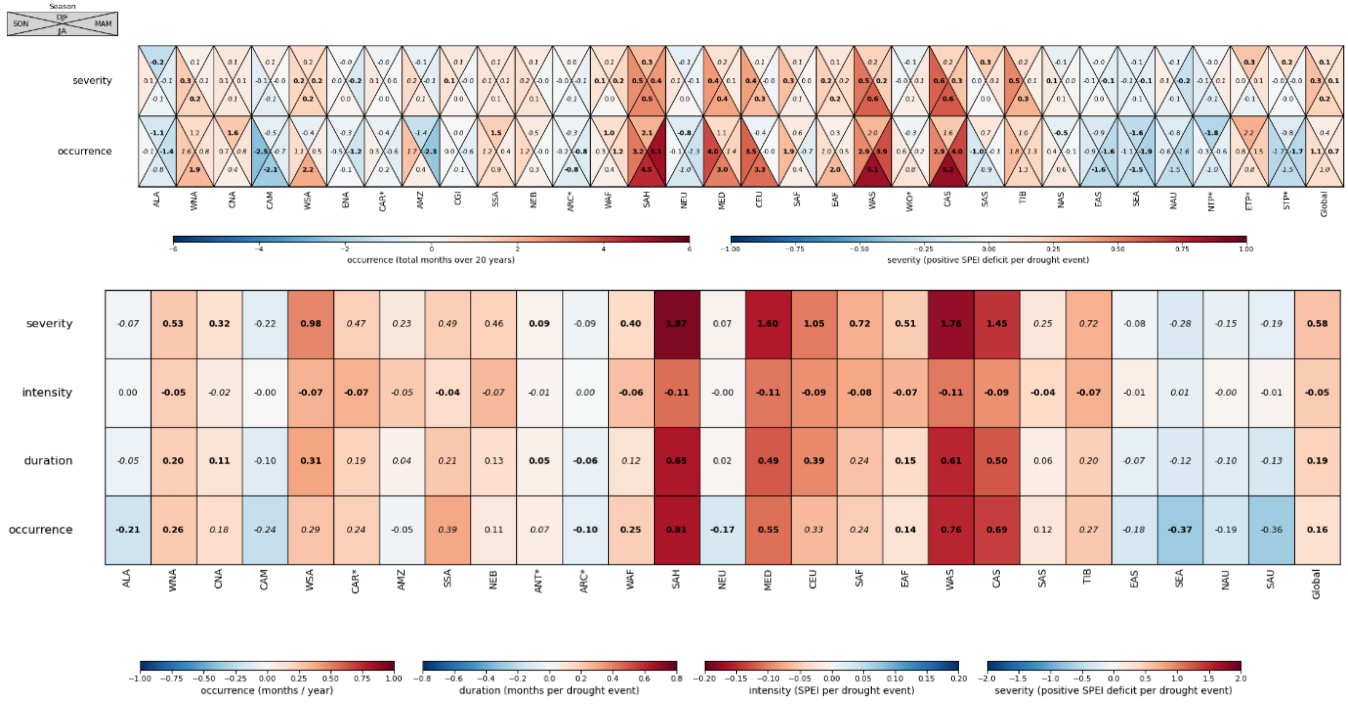

Figure 8: MME regional changes in drought characteristics across IPCC AR6 regions for the 2036–2055 period under NTCF mitigation. The upper panel shows seasonal changes in drought occurrence and severity for DJF, MAM, JJA, and SON; the lower panel shows annual mean changes in occurrence, duration, intensity, and severity. Regional values are calculated as latitude-weighted area means over land grid cells within each IPCC reference region. The global value in the annual panel represents the area-weighted mean across all land grid cells. Bold values indicate changes that are both statistically significant at the 90% level based on a two-tailed Student's t-test and consistent in sign across at least 5 out of 7 models; italic values indicate changes consistent in sign across at least 5 out of 7 models but not meeting the significance threshold.

https://doi.org/10.5194/egusphere-2026-3416
Preprint. Discussion started: 19 June 2026

The Sahel (SAH), West Asia (WAS), and Central Asia (CAS) constitute the primary hotspot regions. In SAH, drought occurrence increases by 4.9–5.8 months per season in MAM and JJA, with significant positive anomalies in all four seasons and an annual mean of +0.8 months yr^{-1}; severity reaches ~1.9 annually, among the most negative values across all regions. WAS shows similarly large and seasonally consistent increases (2.6–5.5 months per season), with the largest severity signal of any region (−0.6 SPEI units in JJA). CAS occurrence increases range from 1.4 months in DJF to 5.2 months in JJA, also significant year-round. The co-occurrence of robust signals across all metrics and all seasons in these three regions points to a near-perennial compounding of already-elevated water stress. The Mediterranean (MED) shows robust annual increases (+0.55 months yr^{-1} occurrence, severity −1.60), peaking in SON (4.2 months), consistent with the well-documented tendency toward summer and autumn drying in this region. Central Europe (CEU) displays a weaker but coherent signal concentrated in JJA and SON.

Among regions experiencing significant drought reductions, Southeast Asia (SEA) records the largest annual decrease (−0.37 months yr^{-1}), with the strongest signal in MAM (−1.8 months) and JJA (−2.4 months), physically consistent with the strengthened Asian summer monsoon. Australia (NAU, SAU) shows reductions of −0.19 and −0.36 months yr^{-1} respectively, present across multiple seasons. Central America (CAM) records −0.24 months yr^{-1} annually, with the largest decreases in JJA and SON (−2.6 months). In all regions where reductions are significant, the signal extends consistently to severity, reinforcing physical consistency.

Seasonally, MAM and JJA dominate as the periods of maximum drought intensification across most land regions, reflecting the compound influence of enhanced PET and reduced precipitation during the pre-monsoon and warm seasons. The prominence of MAM in SAH, WAS, and CAS points to an effective lengthening of the annual dry period in these regions. DJF generally shows the weakest response, though WAS and CAS remain significant even in winter. At the global scale, the area-weighted annual mean shows small but positive occurrence (+0.16 months yr^{-1}) and severity (+0.58) anomalies, reflecting the dominance of drought-intensifying regions in land area over drought-reducing ones.

4 Seasonal changes in exposure to droughts

Population exposure to drought represents the combined influence of climatic stress and demographic distribution, providing an integrated measure of potential human vulnerability to water scarcity. Unlike purely meteorological indices, exposure-based metrics account for both the number of people affected and the duration of drought conditions. Figure 9 shows seasonal changes in population exposure to drought (in million person-months per decade) under NTCF mitigation relative to SSP3-7.0, for JJA and DJF. Increases dominate across most low- and mid-latitude regions in both seasons.

https://doi.org/10.5194/egusphere-2026-3416
Preprint. Discussion started: 19 June 2026

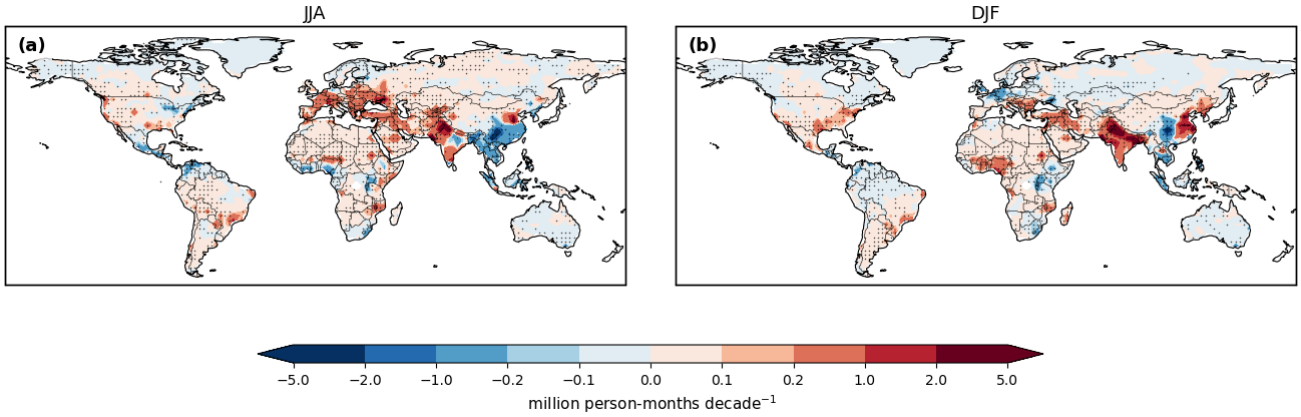

Figure 9: Seasonal changes in gridded population exposure to drought under NTCF mitigation for (a) JJA and (b) DJF during 2036–2055. Stippling indicates regions where at least 5 out of 7 models agree on the sign of the change. Values represent total population exposure within each 2.5° × 2.5° grid cell.

In JJA, the most extensive and robust increases in exposure occur across Europe, the Middle East, and extending eastward into Pakistan/north-western India and Central Asia, with widespread values exceeding 1 million person-months per decade and locally higher values over densely populated areas. More isolated but robust increases are also found over parts of the western United States, southern Brazil, and eastern and south-eastern Africa. By contrast, a coherent and robust reduction in drought exposure is found over South-east and East Asia (in excess of 1 million person-months per decade), consistent with the strengthened monsoon precipitation discussed in previous sections (Fig. S7).

In DJF, the exposure increase over the eastern Mediterranean, Middle East, and western Asia persists, though with somewhat weaker magnitudes than in JJA over most of the domain. A notable exception is the Iran–Pakistan corridor, where the largest exposure increases in the dataset are found, reflecting the combination of large positive drought occurrence anomalies and high population density in this region. Additional increases emerge over the Sahel, parts of Mexico and the eastern United States, and south-eastern Africa. The reduction over East and Southeast Asia contracts compared to JJA but remains visible, with a marked increase over eastern China mostly due to the high population of the region. Increased exposure also spreads across South Asia, particularly over the densely populated Indo-Gangetic plain.

Across seasons, exposure patterns show notable coherence between JJA and SON over Europe, the Mediterranean, and South and East Asia, reflecting the persistence of summer-driven drying into autumn (Fig. S18). MAM and DJF are similarly coherent over the Middle East and northern Africa, where limited seasonal recovery in soil moisture carries drought conditions into the pre-monsoon period.

https://doi.org/10.5194/egusphere-2026-3416
Preprint. Discussion started: 19 June 2026

These pairings indicate that tropical and subtropical exposure is shaped primarily by the persistence of dry-season conditions into the spring, while European and Mediterranean exposure is driven by summer thermal forcing and its seasonal legacy into autumn. A small number of regions stand out as experiencing robust positive exposure anomalies across the majority of the seasons, if not year-round, pointing to a near-permanent intensification of drought risk under NTCF mitigation. The Middle East and the Iran–Pakistan/northwestern India corridor are the clearest examples with increases visible in every season, reflecting the compound effect of large drought occurrence anomalies and high and growing population density. Eastern Europe and the eastern Mediterranean also display a consistent positive signal across all four seasons, though with somewhat lower magnitudes, suggesting that the well-documented summer drying tendency in this region is not confined to the warm season but represents a year-round shift in drought exposure under NTCF mitigation. Parts of the western and eastern United States show a weaker but recurring positive signal across seasons, though largely without stippling, indicating a tendency toward increased exposure that lacks the cross-model robustness seen in the other hotspots.

5 Conclusions

This study investigates the effects of non-methane near-term climate forcer (NTCF) mitigation on future drought risk using multi-model simulations from seven CMIP6 Earth System Models within the AerChemMIP framework. By contrasting the SSP3-7.0 and SSP3-7.0-lowNTCF scenarios, which share identical greenhouse gas trajectories but apply contrasting controls across the full range of non-methane near-term climate forcers, including aerosols and their precursors gases, we isolate the climate signal of NTCF reductions on drought frequency, duration, intensity, and severity across regions and seasons over the period 2036–2055. The SSP3-7.0 scenario is particularly suited for this purpose given its strong forcing contrast and its representativeness of a high-emission; low-mitigation future relevant to near-term impact assessment (Shiogama et al., 2023). This paired scenario design, applied to a large multi-model ensemble, addresses key limitations of prior work, which has largely relied on single-species perturbations, idealised frameworks, or analyses focused on temperature and precipitation alone.

Our main finding is that NTCF mitigation exerts negligible influence on global-mean drought tendency, which is dominated by greenhouse-gas-driven warming and the associated increase in evaporative demand. This result underscores a critical point: global or hemispheric metrics substantially obscure the regional drought hazards that NTCF mitigation can both alleviate and exacerbate. The regional response is strongly heterogeneous and cannot be characterised by a single narrative. The most robust and spatially coherent drought intensification under NTCF mitigation occurs across the Sahel, the Middle East, and Central Asia, where drought occurrence, duration, intensity, and severity all increase significantly across all seasons, pointing to a near-perennial compounding of already-elevated water stress. The Mediterranean and central Europe display similarly robust increases, peaking in boreal summer and autumn. These regions also show the highest population exposure to drought, with

https://doi.org/10.5194/egusphere-2026-3416
Preprint. Discussion started: 19 June 2026

the Iran–Pakistan–north-western India corridor and the eastern Mediterranean exhibiting year-round increases in drought-affected population.

The physical mechanisms underpinning these responses are identified through a combination of water balance diagnostics and large-scale circulation analysis. The spatial patterns of drought change are closely coherent with anomalies in P−PET, with PET increases playing the dominant role across the Northern Hemisphere midlatitudes in summer (~64% of the extratropical P−PET signal in JJA), and precipitation suppression being relatively more important in winter (~57% globally in DJF). Crucially, the drying over remote regions, including the Mediterranean, northern Africa, the Middle East, and the western United States, cannot be attributed to local emission changes alone. We suggest that the large aerosol emission reductions concentrated over South and East Asia are the primary driver of this remote drying, operating through a chain of dynamical responses: the removal of local aerosol cooling displaces and strengthens the Asian monsoon convection, generating circulation anomalies that propagate well beyond the immediate source region to suppress rainfall and enhance evaporative demand across the Mediterranean, northern Africa, the Middle East, and the western United States. In boreal summer, this tropical heating anomaly generates a quasi-stationary Rossby wave train propagating across the Northern Hemisphere midlatitudes, inducing anomalous subsidence and surface warming over Europe and the Middle East. An additional pathway operates through the monsoon-desert mechanism, whereby enhanced monsoonal outflow drives compensating descent over adjacent arid regions including northern Africa and southern Africa. In boreal winter, an analogous but structurally distinct teleconnection is linked to a westward shift of the Walker circulation and changes in the East Asian winter monsoon, with downstream effects on drought occurrence across the Middle East, southwestern Asia, and the western United States. These remote influences explain the synchronised drying across the western US, southern Europe, and the Middle East, emphasising the global reach of regional aerosol forcing changes. These findings directly address the call in the introduction for process-based understanding of how large-scale circulation changes mediate the regional hydrological response to anthropogenic forcing.

A smaller but consistent set of regions, notably Southeast Asia, eastern Australia, northern Europe, and Central America, experience significant reductions in drought occurrence under NTCF mitigation, driven by enhanced precipitation and associated increases in soil moisture. However, the area of robust drought expansion under the SSP3-7.0-lowNTCF scenario exceeds that of drought relief across all seasons, and the beneficial effects tend to be seasonally confined, whereas the drought-intensifying signal is more persistent through the year.

Our analysis of drought characteristics across multiple SPEI timescales reveals a systematic pattern: the drought response intensifies and spatially concentrates as the accumulation period lengthens from 3 to 12 months. While short-term meteorological drought (SPEI-3) responds rapidly to seasonal water balance anomalies, hydrological drought (SPEI-12) accumulates the effects of repeated evaporative and precipitation deficits, producing larger and more spatially coherent anomalies over the Middle East, Central Asia, and southwestern United States. This timescale dependence has direct

https://doi.org/10.5194/egusphere-2026-3416
Preprint. Discussion started: 19 June 2026

implications for adaptation: near-term air quality policies carry differentiated consequences for agricultural drought risk and longer-term hydrological stress, with the latter arguably posing greater challenges for water resource management.

These results demonstrate that while NTCF mitigation delivers clear and well-documented benefits for air quality and, in many regions, for drought risk, it simultaneously and paradoxically intensifies drought conditions in some of the world's most water-stressed and vulnerable regions. This regional asymmetry is physically robust across the model ensemble and arises not from simple thermodynamic responses but from a complex interplay of radiative forcing, land–atmosphere feedbacks, and remote dynamical teleconnections. The concentration of robust drought exposure increases across already water-stressed and densely populated regions, notably the Middle East, eastern Mediterranean, and parts of South Asia, underscores the need for adaptation strategies that are explicitly attentive to vulnerability, and points to an important focus for future work linking NTCF mitigation scenarios to health, food security, and water resource outcomes.

Several important limitations should be noted. The experimental design holds CO_2 and CH_4 emissions constant between scenarios, which isolates the NTCF signal but precludes assessment of synergistic interactions between greenhouse gas and NTCF reductions. The use of the Hargreaves–Samani method for PET estimation does not account for all meteorological controls on evaporative demand. Structural uncertainty in aerosol–chemistry–cloud interactions remain substantial, and higher-resolution simulations will be needed to resolve regional circulation features and land–atmosphere feedbacks more accurately. The assumption of linear superposition of GHG and NTCF forcing merits attention as non-linear aerosol–cloud interactions are likely most significant over regions of largest emission change, particularly South and East Asia, where our estimates may represent an upper bound on the true forced response.

Future research should prioritise joint assessments of greenhouse gas and NTCF mitigation, incorporate higher-resolution regional simulations to better constrain circulation feedbacks, and integrate socio-economic pathways to quantify compound risks to agriculture, water resources, and public health. Ultimately, this study underscores that near-term climate forcer mitigation, while essential for improving air quality and contributing to climate goals, must be coupled with proactive, regionally tailored adaptation strategies in areas where its hydrological consequences are most severe.

https://doi.org/10.5194/egusphere-2026-3416
Preprint. Discussion started: 19 June 2026

Code and data availability

SPEI-based drought metrics were calculated using the Climpact framework (https://github.com/ARCCSS-extremes/climpact) and the SPEI R package following Vicente-Serrano et al. (2010). Analysis scripts are available from the corresponding author upon request.

The CMIP6 model simulations used in this study are available from the Earth System Grid Federation (ESGF; https://esgf-node.llnl.gov/search/cmip6/). Regional analyses were based on the IPCC reference regions shapefile, available from https://github.com/SantanderMetGroup/ATLAS. Population exposure was calculated using the Gridded Population of the World, Version 4 (GPWv4) population count adjusted to match the 2015 Revision of UN WPP country totals, Revision 11, available from NASA SEDAC / Earthdata (https://www.earthdata.nasa.gov/data/catalog/sedac-ciesin-sedac-gpwv4-apct-wpp-2015-r11-4.11). The land mask was derived from the NASA GPM IMERG land-sea mask NetCDF file (https://gpm.nasa.gov/data/directory/imerg-land-sea-mask-netcdf), with land defined as grid cells with water surface coverage no greater than 15%.

Author contributions

TZ and MAB designed the study. TZ carried out the analysis and wrote the original draft of the manuscript. TZ and MAB discussed the results and interpreted the findings. MAB supervised the project and revised the manuscript throughout its development. DS contributed to the scientific interpretation and reviewed the manuscript.

Competing interests

The authors declare that they have no conflicts of interest.

Acknowledgements

The authors acknowledge the World Climate Research Programme, which coordinated and promoted CMIP6, and thank the climate modelling groups for producing and making available their model output. We also acknowledge the providers of the GPWv4 population dataset, the IPCC reference region shapefile, and the NASA GPM IMERG land-sea mask used in this study.

https://doi.org/10.5194/egusphere-2026-3416
Preprint. Discussion started: 19 June 2026

Financial support

We acknowledge support from the UK Natural Environment Research Council (NERC) grant NE/N006038/1.

References

Aas, W., Mortier, A., Bowersox, V., Cherian, R., Faluvegi, G., Fagerli, H., Hand, J., Klimont, Z., Galy-Lacaux, C., Lehmann, C. M. B., Myhre, C. L., Myhre, G., Olivié, D., Sato, K., Quaas, J., Rao, P. S. P., Schulz, M., Shindell, D., Skeie, R. B., Stein, A., Takemura, T., Tsyro, S., Vet, R., and Xu, X.: Global and regional trends of atmospheric sulfur, Sci. Rep., 9, 953, https://doi.org/10.1038/s41598-018-37304-0, 2019.

Allen, R. J., Horowitz, L. W., Naik, V., Oshima, N., O'Connor, F. M., Turnock, S., Shim, S., Sager, P. L., Van Noije, T., Tsigaridis, K., Bauer, S. E., Sentman, L. T., John, J. G., Broderick, C., Deushi, M., Folberth, G. A., Fujimori, S., and Collins, W. J.: Significant climate benefits from near-term climate forcer mitigation in spite of aerosol reductions, Environ. Res. Lett., 16, 034010, https://doi.org/10.1088/1748-9326/abe06b, 2021.

Allen, R. J., Turnock, S., Nabat, P., Neubauer, D., Lohmann, U., Olivié, D., Oshima, N., Michou, M., Wu, T., Zhang, J., Takemura, T., Schulz, M., Tsigaridis, K., Bauer, S. E., Emmons, L., Horowitz, L., Naik, V., van Noije, T., Bergman, T., Lamarque, J.-F., Zanis, P., Tegen, I., Westervelt, D. M., Le Sager, P., Good, P., Shim, S., O'Connor, F., Akritidis, D., Georgoulias, A. K., Deushi, M., Sentman, L. T., John, J. G., Fujimori, S., and Collins, W. J.: Climate and air quality impacts due to mitigation of non-methane near-term climate forcers, Atmos. Chem. Phys., 20, 9641–9663, https://doi.org/10.5194/acp-20-9641-2020, 2020.

Ban-Weiss, G. A., Cao, L., Bala, G., and Caldeira, K.: Dependence of climate forcing and response on the altitude of black carbon aerosols, Clim. Dynam., 38, 897–911, https://doi.org/10.1007/s00382-011-1052-y, 2012.

Beguería, S., Vicente-Serrano, S. M., Reig, F., and Latorre, B.: Standardized precipitation evapotranspiration index (SPEI) revisited: parameter fitting, evapotranspiration models, tools, datasets and drought monitoring, Int. J. Climatol., 34, 3001–3023, https://doi.org/10.1002/joc.3887, 2013.

Bollasina, M. A., Ming, Y., and Ramaswamy, V.: Anthropogenic aerosols and the weakening of the South Asian summer monsoon, Science, 334, 502–505, https://doi.org/10.1126/science.1204994, 2011.

Boucher, O., Randall, D., Artaxo, P., Bretherton, C., Feingold, G., Forster, P., Kerminen, V.-M., Kondo, Y., Liao, H., Lohmann, U., Rasch, P., Satheesh, S. K., Sherwood, S., Stevens, B., and Zhang, X. Y.: Clouds and aerosols, in: Climate Change 2013: The Physical Science Basis. Contribution of Working Group I to the Fifth Assessment Report of the Intergovernmental Panel on Climate Change, edited by: Stocker, T. F., Qin, D., Plattner, G.-K., Tignor, M., Allen, S. K., Boschung, J., Nauels, A., Xia, Y., Bex, V., and Midgley, P. M., Cambridge University Press, Cambridge, UK and New York, NY, USA, 571–657, https://doi.org/10.1017/CBO9781107415324.016, 2013.

Buchholz, R. R., Worden, H. M., Park, M., Francis, G., Deeter, M. N., Edwards, D. P., Emmons, L. K., Gaubert, B., Gille, J., Martínez-Alonso, S., Tang, W., Kumar, R., Drummond, J. R., Clerbaux, C., George, M., Coheur, P.-F., Hurtmans, D.,

https://doi.org/10.5194/egusphere-2026-3416
Preprint. Discussion started: 19 June 2026

Bowman, K. W., Luo, M., Payne, V. H., Worden, J. R., Chin, M., Levy, R. C., Warner, J., Wei, Z., and Kulawik, S. S.: Air pollution trends measured from Terra: CO and AOD over industrial, fire-prone, and background regions, Remote Sens. Environ., 256, 112275, https://doi.org/10.1016/j.rse.2020.112275, 2021.

Center for International Earth Science Information Network (CIESIN): Gridded Population of the World, Version 4 (GPWv4): Population Count Adjusted to Match the 2015 Revision of UN WPP Country Totals, Revision 11, NASA Socioeconomic Data and Applications Center (SEDAC) [data set], https://doi.org/10.7927/H4PN93PB, 2018.

Cherchi, A., Annamalai, H., Masina, S., Navarra, A., and Alessandri, A.: Twenty-first century projected June–September climate change in the Mediterranean and Middle East and the associated atmospheric circulation changes, J. Climate, 29, 2441–2456, https://doi.org/10.1175/JCLI-D-15-0339.1, 2016.

Christidis, N., Jones, G. S., and Stott, P. A.: Dramatically increasing chance of extremely hot summers since the 2003 European heatwave, Nat. Clim. Change, 5, 46–50, https://doi.org/10.1038/nclimate2468, 2015.

Chung, E.-S. and Soden, B. J.: Hemispheric climate shifts driven by anthropogenic aerosol–cloud interactions, Nat. Geosci., 10, 566–571, https://doi.org/10.1038/ngeo2988, 2017.

Collins, W. J., Lamarque, J.-F., Schulz, M., Boucher, O., Eyring, V., Hegglin, M. I., Maycock, A., Myhre, G., Prather, M., Shindell, D., and Smith, S. J.: AerChemMIP: quantifying the effects of chemistry and aerosols in CMIP6, Geosci. Model Dev., 10, 585–607, https://doi.org/10.5194/gmd-10-585-2017, 2017.

Cook, B. I., Mankin, J. S., and Anchukaitis, K. J.: Climate change and drought: from past to future, Curr. Clim. Change Rep., 4, 164–179, https://doi.org/10.1007/s40641-018-0093-2, 2018.

De Sousa Lima, J. R., Antonino, A. C. D., De Souza, E. S., Hammecker, C., Montenegro, S. M. G. L., and De Oliveira Lira, C. A. B.: Calibration of Hargreaves-Samani equation for estimating reference evapotranspiration in sub-humid region of Brazil, J. Water Resour. Prot., 5, 1–5, https://doi.org/10.4236/jwarp.2013.512a001, 2013.

Diffenbaugh, N. S., Singh, D., Mankin, J. S., Horton, D. E., Swain, D. L., Bhattacharya, A., Tsiang, M., Haugen, M., and Shearer, E. J.: Quantifying the influence of global warming on unprecedented extreme climate events, P. Natl. Acad. Sci. USA, 114, 4881–4886, https://doi.org/10.1073/pnas.1618082114, 2017.

Diffenbaugh, N. S., Swain, D. L., and Touma, D.: Anthropogenic warming has increased drought risk in California, P. Natl. Acad. Sci. USA, 112, 3931–3936, https://doi.org/10.1073/pnas.1422385112, 2015.

Ebi, K. L., Vanos, J., Baldwin, J. W., Bell, J. E., Hondula, D. M., Errett, N. A., Hayes, K., Reid, C. E., Saha, S., Spector, J., and Berry, P.: Extreme weather and climate change: population health and health system implications, Annu. Rev. Publ. Health, 42, 293–315, https://doi.org/10.1146/annurev-publhealth-012420-105026, 2021.

Eyring, V., Bony, S., Meehl, G. A., Senior, C. A., Stevens, B., Stouffer, R. J., and Taylor, K. E.: Overview of the Coupled Model Intercomparison Project Phase 6 (CMIP6) experimental design and organization, Geosci. Model Dev., 9, 1937–1958, https://doi.org/10.5194/gmd-9-1937-2016, 2016.

https://doi.org/10.5194/egusphere-2026-3416
Preprint. Discussion started: 19 June 2026

GBD 2021 Risk Factors Collaborators: Global burden and strength of evidence for 88 risk factors in 204 countries and 811 subnational locations, 1990–2021: a systematic analysis for the Global Burden of Disease Study 2021, Lancet, 403, 2162–2203, https://doi.org/10.1016/S0140-6736(24)00933-4, 2024.

Haines, A., Amann, M., Borgford-Parnell, N., Leonard, S., Kuylenstierna, J., and Shindell, D.: Short-lived climate pollutant mitigation and the Sustainable Development Goals, Nat. Clim. Change, 7, 843–849, https://doi.org/10.1038/s41558-017-0012-x, 2017.

Hargreaves, G. H. and Samani, Z. A.: Reference crop evapotranspiration from temperature, Appl. Eng. Agric., 1, 96–99, https://doi.org/10.13031/2013.26773, 1985.

Held, I. M. and Soden, B. J.: Robust responses of the hydrological cycle to global warming, J. Climate, 19, 5686–5699, https://doi.org/10.1175/JCLI3990.1, 2006.

Hoesly, R. M., Smith, S. J., Feng, L., Klimont, Z., Janssens-Maenhout, G., Pitkanen, T., Seibert, J. J., Vu, L., Andres, R. J., Bolt, R. M., Bond, T. C., Dawidowski, L., Kholod, N., Kurokawa, J., Li, M., Liu, L., Lu, Z., Moura, M. C. P., O'Rourke, P. R., and Zhang, Q.: Historical (1750–2014) anthropogenic emissions of reactive gases and aerosols from the Community Emissions Data System (CEDS), Geosci. Model Dev., 11, 369–408, https://doi.org/10.5194/gmd-11-369-2018, 2018.

Howitt, R. E., MacEwan, D., Medellín-Azuara, J., Lund, J. R., and Sumner, D. A.: Economic Analysis of the 2015 Drought for California Agriculture, Center for Watershed Sciences, University of California – Davis, Davis, CA, USA, 16 pp., 2015.

Kwon, M. and Sung, J. H.: Changes in future drought with HadGEM2-AO projections, Water, 11, 312, https://doi.org/10.3390/w11020312, 2019.

Lei, Y., Yue, X., Liao, H., Zhang, L., Zhou, H., Tian, C., Gong, C., Ma, Y., Cao, Y., Seco, R., Karl, T., and Potosnak, M.: Global perspective of drought impacts on ozone pollution episodes, Environ. Sci. Technol., 56, 3932–3940, https://doi.org/10.1021/acs.est.1c07260, 2022.

Lelieveld, J., Haines, A., Burnett, R., et al.: Air pollution deaths attributable to fossil fuels: observational and modelling study, BMJ, 383, e077784, https://doi.org/10.1136/bmj-2023-077784, 2023.

Lelieveld, J., Klingmüller, K., Pozzer, A., Burnett, R. T., Haines, A., and Ramanathan, V.: Effects of fossil fuel and total anthropogenic emission removal on public health and climate, P. Natl. Acad. Sci. USA, 116, 7192–7197, https://doi.org/10.1073/pnas.1819989116, 2019.

Liu, W., Sun, F., Lim, W. H., Zhang, J., Wang, H., Shiogama, H., and Zhang, Y.: Global drought and severe drought-affected populations in 1.5 and 2 °C warmer worlds, Earth Syst. Dynam., 9, 267–283, https://doi.org/10.5194/esd-9-267-2018, 2018.

Liu, Y., Cai, W., Sun, C., Song, H., Cobb, K. M., Li, J., Leavitt, S. W., Wu, L., Cai, Q., Liu, R., Ng, B., Cherubini, P., Büntgen, U., Song, Y., Wang, G., Lei, Y., Yan, L., Li, Q., Ma, Y., Fang, C., Sun, J., Li, X., Chen, D., and Linderholm, H. W.: Anthropogenic aerosols cause recent pronounced weakening of Asian Summer Monsoon relative to last four centuries, Geophys. Res. Lett., 46, 5469–5479, https://doi.org/10.1029/2019GL082497, 2019.

Liu, Z., Bollasina, M. A., and Wilcox, L. J.: Impact of Asian aerosols on the summer monsoon strongly modulated by regional precipitation biases, Atmos. Chem. Phys., 24, 7227–7252, https://doi.org/10.5194/acp-24-7227-2024, 2024.

https://doi.org/10.5194/egusphere-2026-3416
Preprint. Discussion started: 19 June 2026

Lloyd-Hughes, B. and Saunders, M. A.: A drought climatology for Europe, Int. J. Climatol., 22, 1571–1592, https://doi.org/10.1002/joc.846, 2002.

Lynch, K. M., Lyles, R. H., Waller, L. A., Abadi, A. M., Bell, J. E., and Gribble, M. O.: Drought severity and all-cause mortality rates among adults in the United States: 1968–2014, Environ. Health, 19, 52, https://doi.org/10.1186/s12940-020-00597-8, 2020.

McKee, T. B., Doesken, N. J., and Kleist, J.: The relationship of drought frequency and duration to time scales, in: Proceedings of the 8th Conference on Applied Climatology, Anaheim, California, 17–22 January 1993, American Meteorological Society, Boston, MA, 179–184, 1993.

Ming, Y., Ramaswamy, V., and Persad, G.: Two opposing effects of absorbing aerosols on global-mean precipitation, Geophys. Res. Lett., 37, L13701, https://doi.org/10.1029/2010GL042895, 2010.

Miyazaki, K., Eskes, H., Sudo, K., Boersma, K. F., Bowman, K., and Kanaya, Y.: Decadal changes in global surface NOx emissions from multi-constituent satellite data assimilation, Atmos. Chem. Phys., 17, 807–837, https://doi.org/10.5194/acp-17-807-2017, 2017.

Moseid, K. O., Schulz, M., Storelvmo, T., Julsrud, I. R., Olivié, D., Nabat, P., Wild, M., Cole, J. N. S., Takemura, T., Oshima, N., Bauer, S. E., and Gastineau, G.: Bias in CMIP6 models as compared to observed regional dimming and brightening, Atmos. Chem. Phys., 20, 16023–16040, https://doi.org/10.5194/acp-20-16023-2020, 2020.

Myhre, G., Shindell, D., Bréon, F.-M., Collins, W., Fuglestvedt, J., Huang, J., Koch, D., Lamarque, J.-F., Lee, D., Mendoza, B., Nakajima, T., Robock, A., Stephens, G., Takemura, T., and Zhang, H.: Anthropogenic and natural radiative forcing, in: Climate Change 2013: The Physical Science Basis. Contribution of Working Group I to the Fifth Assessment Report of the Intergovernmental Panel on Climate Change, edited by: Stocker, T. F., Qin, D., Plattner, G.-K., Tignor, M., Allen, S. K., Boschung, J., Nauels, A., Xia, Y., Bex, V., and Midgley, P. M., Cambridge University Press, Cambridge, UK, 659–740, https://doi.org/10.1017/CBO9781107415324.018, 2013.

Naimark, J. G., Fiore, A. M., Jin, X., Wang, Y., Klovenski, E., and Braneon, C.: Evaluating drought responses of surface ozone precursor proxies: variations with land cover type, precipitation, and temperature, Geophys. Res. Lett., 48, e2020GL091520, https://doi.org/10.1029/2020GL091520, 2021.

Ogunrinde, A. T., Emmanuel, I., Enaboifo, M. A., Ajayi, T. A., and Pham, Q. B.: Spatio-temporal calibration of Hargreaves–Samani model in the northern region of Nigeria, Theor. Appl. Climatol., 147, 1213–1228, https://doi.org/10.1007/s00704-021-03897-2, 2021.

Polson, D., Bollasina, M. A., Hegerl, G. C., and Wilcox, L. J.: Decreased monsoon precipitation in the Northern Hemisphere due to anthropogenic aerosols, Geophys. Res. Lett., 41, 6023–6029, https://doi.org/10.1002/2014GL060811, 2014.

Richardson, T. B., Forster, P. M., Andrews, T., and Parker, D. J.: Drivers of precipitation change: An energetic understanding, J. Climate, 31, 9641–9657, https://doi.org/10.1175/JCLI-D-17-0240.1, 2018.

Rodwell, M. J. and Hoskins, B. J.: Monsoons and the dynamics of deserts, Q. J. Roy. Meteor. Soc., 122, 1385–1404, https://doi.org/10.1002/qj.49712253408, 1996.

https://doi.org/10.5194/egusphere-2026-3416
Preprint. Discussion started: 19 June 2026

Salzmann, M.: Global warming without global mean precipitation increase?, Science Advances, 2, e1501572, https://doi.org/10.1126/sciadv.1501572, 2016.

Samset, B. H., Sand, M., Smith, C. J., Bauer, S. E., Forster, P. M., Fuglestvedt, J. S., Osprey, S., and Schleussner, C.-F.: Climate impacts from a removal of anthropogenic aerosol emissions, Geophys. Res. Lett., 45, 1020–1029, https://doi.org/10.1002/2017GL076079, 2018.

Seneviratne, S. I., Nicholls, N., Easterling, D., Goodess, C. M., Kanae, S., Kossin, J., Luo, Y., Marengo, J., McInnes, K., Rahimi, M., Reichstein, M., Sorteberg, A., Vera, C., and Zhang, X.: Changes in climate extremes and their impacts on the natural physical environment, in: Managing the Risks of Extreme Events and Disasters to Advance Climate Change Adaptation. A Special Report of Working Groups I and II of the Intergovernmental Panel on Climate Change (IPCC), edited by: Field, C. B., Barros, V., Stocker, T. F., Qin, D., Dokken, D. J., Ebi, K. L., Mastrandrea, M. D., Mach, K. J., Plattner, G.-K., Allen, S. K., Tignor, M., and Midgley, P. M., Cambridge University Press, Cambridge, UK, and New York, NY, USA, 109–230, https://doi.org/10.1017/CBO9781139177245.006, 2012.

Shiogama, H., Fujimori, S., Hasegawa, T., et al.: Important distinctiveness of SSP3–7.0 for use in impact assessments, Nat. Clim. Chang., 13, 1276–1278, https://doi.org/10.1038/s41558-023-01883-2, 2023.

Song, F., Zhou, T., and Qian, Y.: Responses of East Asian summer monsoon to natural and anthropogenic forcings in the 17 latest CMIP5 models, Geophys. Res. Lett., 41, 596–603, https://doi.org/10.1002/2013GL058705, 2014.

Stjern, C. W., Samset, B. H., Myhre, G., Forster, P. M., Hodnebrog, Ø., Andrews, T., Boucher, O., Faluvegi, G., Iversen, T., Kasoar, M., Kharin, V., Kirkevåg, A., Lamarque, J.-F., Olivié, D., Richardson, T., Shawki, D., Shindell, D., Smith, C. J., Takemura, T., and Voulgarakis, A.: Rapid adjustments cause weak surface temperature response to increased black carbon concentrations, J. Geophys. Res.-Atmos., 122, 11462–11481, https://doi.org/10.1002/2017JD027326, 2017.

Szopa, S., Naik, V., Adhikary, B., Artaxo, P., Berntsen, T., Collins, W. D., Fuzzi, S., Gallardo, L., Kiendler-Scharr, A., Klimont, Z., Liao, H., Unger, N., and Zanis, P.: Short-lived climate forcers, in: Climate Change 2021: The Physical Science Basis. Contribution of Working Group I to the Sixth Assessment Report of the Intergovernmental Panel on Climate Change, edited by: Masson-Delmotte, V., Zhai, P., Pirani, A., Connors, S. L., Péan, C., Berger, S., Caud, N., Chen, Y., Goldfarb, L., Gomis, M. I., Huang, M., Leitzell, K., Lonnoy, E., Matthews, J. B. R., Maycock, T. K., Waterfield, T., Yelekçi, O., Yu, R., and Zhou, B., Cambridge University Press, Cambridge, UK and New York, NY, USA, 817–922, https://doi.org/10.1017/9781009157896.008, 2021.

Trenberth, K. E., Dai, A., van der Schrier, G., Jones, P. D., Barichivich, J., Briffa, K. R., and Sheffield, J.: Global warming and changes in drought, Nat. Clim. Change, 4, 17–22, https://doi.org/10.1038/nclimate2067, 2014.

Turnock, S. T., Allen, R. J., Archibald, A. T., Dalvi, M., Folberth, G. A., Griffiths, P. T., Keeble, J., Robertson, E., and O'Connor, F. M.: The future climate and air quality response from different near-term climate forcer, climate, and land-use scenarios using UKESM1, Earth's Future, 10, e2022EF002687, https://doi.org/10.1029/2022EF002687, 2022.

Um, M.-J., Kim, Y., Park, D., and Kim, J.: Effects of different reference periods on drought index estimations from 1901 to 2014, Hydrol. Earth Syst. Sci., 21, 4989–5007, https://doi.org/10.5194/hess-21-4989-2017, 2017.

https://doi.org/10.5194/egusphere-2026-3416
Preprint. Discussion started: 19 June 2026

Undorf, S., Polson, D., Bollasina, M. A., Ming, Y., Schurer, A., and Hegerl, G. C.: Detectable impact of local and remote anthropogenic aerosols on the 20th century changes of West African and South Asian monsoon precipitation, J. Geophys. Res.-Atmos., 123, 4871–4889, https://doi.org/10.1029/2017JD027711, 2018.

UNISDR and CRED: The Human Cost of Weather-Related Disasters 1995–2015, United Nations Office for Disaster Risk Reduction and Centre for Research on the Epidemiology of Disasters, Geneva, 2015.

Vicente-Serrano, S. M., Beguería, S., and López-Moreno, J. I.: A multiscalar drought index sensitive to global warming: the Standardized Precipitation Evapotranspiration Index, J. Climate, 23, 1696–1718, https://doi.org/10.1175/2009JCLI2909.1, 2010.

Wang, T., Tu, X., Singh, V. P., Chen, X., and Lin, K.: Global data assessment and analysis of drought characteristics based on CMIP6, J. Hydrol., 596, 126091, https://doi.org/10.1016/j.jhydrol.2021.126091, 2021.

Wang, W., Wang, J., and Romanowicz, R.: Uncertainty in SPI calculation and its impact on drought assessment in different climate regions over China, J. Hydrometeorol., 22, 1369–1384, https://doi.org/10.1175/JHM-D-20-0256.1, 2021.

Wells, N., Goddard, S., and Hayes, M. J.: A self-calibrating Palmer Drought Severity Index, J. Climate, 17, 2335–2351, https://doi.org/10.1175/1520-0442(2004)017<2335:ASPDSI>2.0.CO;2, 2004.

Wilcox, L. J., Liu, Z., Samset, B. H., Hawkins, E., Lund, M. T., Nordling, K., Undorf, S., Bollasina, M., Ekman, A. M. L., Krishnan, S., Merikanto, J., and Turner, A. G.: Accelerated increases in global and Asian summer monsoon precipitation from future aerosol reductions, Atmos. Chem. Phys., 20, 11955–11977, https://doi.org/10.5194/acp-20-11955-2020, 2020.

Wilhite, D. A. and Glantz, M. H.: Understanding the drought phenomenon: the role of definitions, Water Int., 10, 111–120, https://doi.org/10.1080/02508068508686328, 1985.

Wu, P., Christidis, N., and Stott, P.: Anthropogenic impact on Earth's hydrological cycle, Nat. Clim. Change, 3, 807–810, https://doi.org/10.1038/nclimate1932, 2013.

Yevjevich, V.: An objective approach to definitions and investigations of continental hydrologic droughts, J. Hydrol., 7, 353, https://doi.org/10.1016/0022-1694(69)90110-3, 1969.

Zhang, S., Stier, P., Dagan, G., and Wang, M.: Anthropogenic aerosols modulated 20th-century Sahel rainfall variability via their impacts on North Atlantic sea surface temperature, Geophys. Res. Lett., 49, e2021GL095629, https://doi.org/10.1029/2021GL095629, 2022.

Zheng, B., Tong, D., Li, M., Liu, F., Hong, C., Geng, G., Li, H., Li, X., Peng, L., Qi, J., Yan, L., Zhang, Y., Zhao, H., Zheng, Y., He, K., and Zhang, Q.: Trends in China's anthropogenic emissions since 2010 as the consequence of clean air actions, Atmos. Chem. Phys., 18, 14095–14111, https://doi.org/10.5194/acp-18-14095-2018, 2018.